5. STUDIES ON FARNESYLTRANSFERASE INHIBITORS

5.1 3D-QSAR studies on benzonitrile derivatives as Farnesyltransferase Inhibitors: A Comparative Molecular Field Analysis approach

5.1.1 Experimental

5.1.1.1 Data set and alignment rules

A series of benzonitrile derivatives have been reported[1] as selective farnesyltransferase (FTase) inhibitors and tested against recombinant human FTase. The *in vitro* activity of compounds inhibiting FTase was determined by using scintillation proximity assay. Rationally selected training and test set provided a means for the development of reliable validated QSAR models. **Table 5.1.1 and 5.1.2** defines the structures and biological activities of training set (**1-34** molecules) and test set (**35-42**) molecules, respectively.

Table 5.1.1 Structures and biological activities of the molecules used in the training set

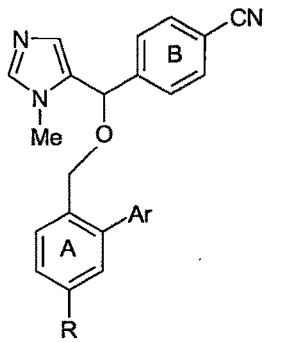

C.N	R	Ar	pIC_{50}
1	Cl	2-ClPh	5.05
2	Cl	3-ClPh	6.09
3	Cl	3-OEtPh	5.95
4	CN	Ph	5.88
5	CN	1-Napthyl	6.02
6	CN	3-ClPh	6.06
7	CN	3-OMePh	6.45
8	CN	3,4-OCH_2OPh	6.06
9	CN	3,4-OCF_2OPh	5.95

10	CN	3-OEtPh	6.16
11	CN	4-OMePh	6.01
12	CN	4-OEtPh	5.92
13	CN	3-OCF_3Ph	6.07
14	CN	4-CH_3Ph	5.95
15	CN	3,5-DiFPh	6.0
16	NO_2	3-OMePh	5.95
17	$NHSO_2CH_3$	3-OMePh	4.45
18	$NHCOCH_2OMe$	3-OMePh	4.95
19	CO_2Me	3-OMePh	4.88
20	CHO	3-OMePh	5.79

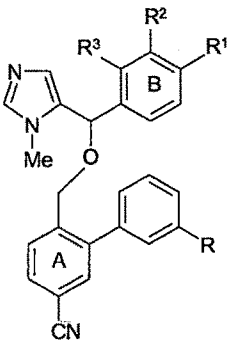

C.N	R	R^1	R^2	R^3	pIC_{50}
21	OMe	Cl	H	H	5.69
22	OMe	CN	Cl	H	6.01
23	Cl	CN	F	H	6.35
24	Cl	CN	H	F	6.11
25	Cl	CF3	H	H	5.95

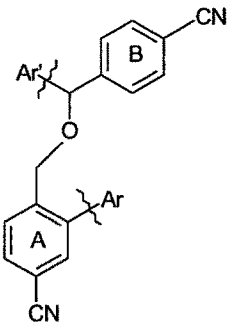

C.N	Ar'	Ar	pIC_{50}
26	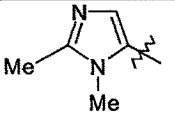	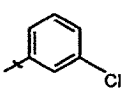	5.69

27	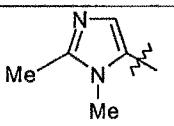	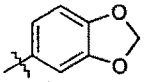	5.79
28		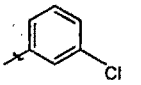	5.39
29	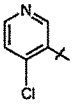	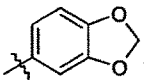	4.82

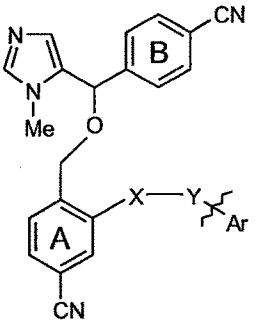

C.N	X-Y	Ar	pIC_{50}
30	$NHSO_2$	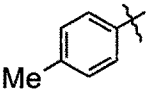	6.0
31	$NHSO_2$	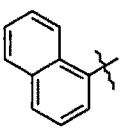	5.58
32	$NHCH_2$	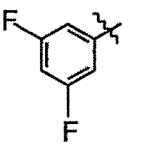	6.21
33	CONH	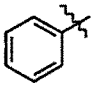	5.65
34	CONH	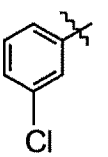	6.12

Table 5.1.2 Structures and biological activities of the molecules used in test set.

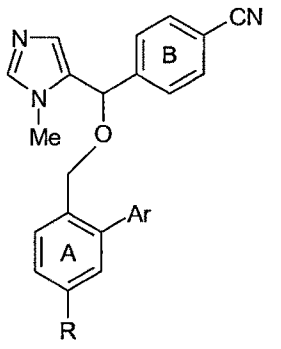

C.N	R	Ar	pIC_{50}
35	Cl	4-Cl-Ph	5.31
36	Cl	3-OMe-Ph	6.04
37	CN	8-Quinolinyl	5.28
38	CN	3-CH_2-OCH_3-Ph	6.72
39	NH_2	3-OMe-Ph	4.39
40	CO_2H	3-OMe-Ph	4.08

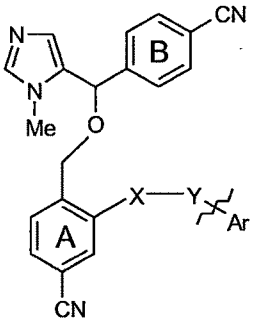

C.N	X-Y	Ar	pIC_{50}
41	$NHSO_2$	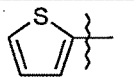	6.05
42	NHCO	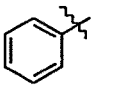	5.30

Alignment rule

The atoms/centroids used for alignments are defined in **Figure 5.1.1**. Superimposition of the molecules is shown in **Figure 5.1.2**. These alignments were subsequently used in CoMFA probe interaction energy calculations.

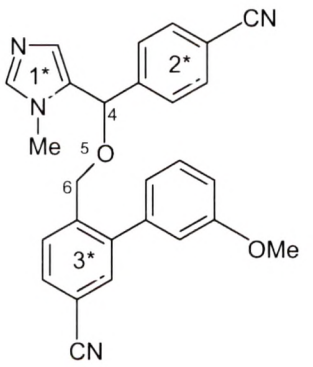

Alignments	Model No.	Atoms / Centroids
I	1	1* 2* 3*
II	2	1* 2* 3* 5
III	3	4 5 6
IV	4	1* 2* 3* 4 5 6

Figure 5.1.1 Alignment rules with template (molecule **7**)

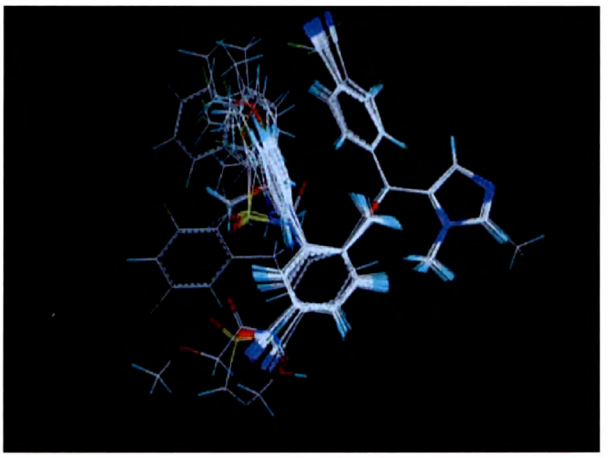

Figure 5.1.2 Alignment of the compounds used in the training set of 3D-QSAR analysis

5.1.2 Results and discussion

3D QSAR studies were performed employing the most commonly used and effective technique COMFA on a series of benzonitrile derivatives **(Table 5.1.1 and 5.1.2)**. **Figures 5.1.1 and 5.1.2** display the alignment rules employed and the superimposition of molecules under study, respectively.

CoMFA results obtained from four different alignments using 34 molecules in training set are shown in **Table 5.1.3**. The CoMFA model generated from shape-based RMS alignment I (Model 1) showed cross-validated r^2 0.408 with two components, non cross-validated r^2 0.965, F value 90.23, bootstrapped r^2 0.982 and predictive r^2 0.450. The steric and electrostatic contributions were 44.5 % and 55.5 %, respectively.

The CoMFA model generated from atom and shape based RMS alignment II (Model 2) **(Table 5.1.3)** showed cross-validated r^2 of 0.307 with two components, non cross-validated r^2 0.954, F value 73.78, bootstrapped r^2 0.971 and predictive r^2 0.350 with 40.9 % steric and 59.1 % electrostatic contributions.

The atom-based alignment III (Model 3) yielded **(Table 5.1.3)** cross-validated r^2 0.299 with two components, non cross-validated r^2 0.971, F value 120.64, bootstrapped r^2 0.984 and predictive r^2 0.30. The steric and electrostatic contributions were 40.3 % and 59.7 %, respectively.

The database alignment IV (Model 4) yielded a cross-validated r^2 of 0.619 with three components, non cross-validated r^2 0.991, F value 249.67, bootstrapped r^2 0.998 and predictive r^2 0.770. The steric and electrostatic contributions were 40.1 % and 59.9 %, respectively. Based on the predictive ability of the four CoMFA models **(Table 5.1.3)**, Model 4 generated with database alignment IV carrying good predictive r^2 (0.770) was selected for developing CoMFA contours.

Table 5.1.3 Results of CoMFA analysis using different alignment rules

Statistical parameters	Alignments			
	I [a]	II [b]	III [c]	IV [d]
r^2_{cv} [e]	0.408	0.307	0.299	**0.619**
N_c [f]	2	2	2	**3**
SEP [g]	0.334	0.324	0.386	**0.284**
r^2_{ncv} [h]	0.965	0.954	0.971	**0.991**
SEE [i]	0.091	0.110	0.087	**0.049**
F value	90.23	73.78	120.64	**249.67**
Prob $r^2 = 0$	0.0	0.0	0.0	**0.0**
r^2_{bs} [j]	0.982	0.971	0.984	**0.998**
S D [k]	0.011	0.016	0.015	**0.018**
r^2_{pred}	0.450	0.350	0.300	**0.770**
Contrib. steric	44.5	40.9	40.3	**40.1**
Contrib. elect	55.5	59.1	59.7	**59.9**

[a] Alignment by shape-based RMS fit; [b] Alignment by atom and shape based RMS fit; [c] Alignment by atom based RMS fit; [d] Alignment by atom and shape-based RMS fit; [e] Cross-validared r^2 ; [f] Number of components; [g] Standard error of prediction; [h] Non cross-validated r^2; [i] Standard error of estimate; [j] boot trapped correlation coefficient obtained from 100 bootstrapping runs; [k] Standard deviation.

The graphs of actual *versus* fitted/predicted activities for the training and test set of molecules are depicted in **Figures 5.1.3 and 5.1.6,** respectively. The field values generated at each grid point were calculated as the scalar product of the associated QSAR coefficient and the standard deviation of all values in the corresponding column of the data table (STD*COEFF) plotted as the percentage contributions to QSAR equation. The CoMFA steric and electrostatic contour maps are shown in **Figures 5.1.4 and 5.1.5,** respectively. The green colored regions indicate areas where steric bulk enhances farnesyltransferase inhibitory activity, while the yellow contours indicate

regions where steric bulk is detrimental for biological activity. Blue colored regions show areas where electropositive charged groups enhance farnesyltransferase inhibitory activity, while red regions represent where electronegative charged groups improve the activity.

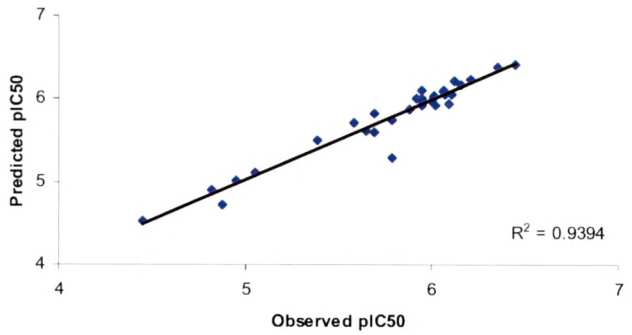

Figure 5.1.3 Graph of observed activity *versus* predicted activities of training set molecules from CoMFA analysis (Model 4); activity expressed as pIC_{50}

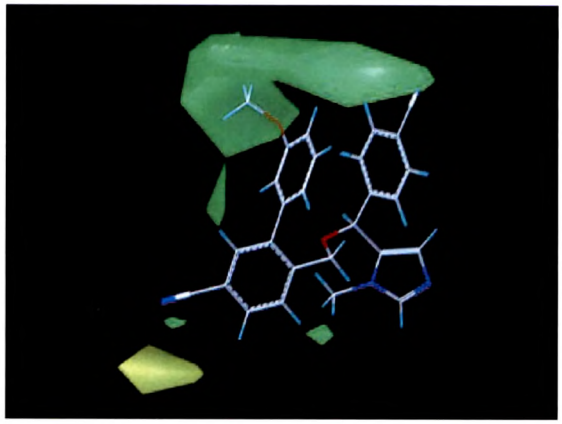

Figure 5.1.4 CoMFA standard deviation coefficient steric contour plots with compound **7**; green contours indicate regions where bulky group increases activity, whereas yellow contour indicates regions where bulky group decreases activity.

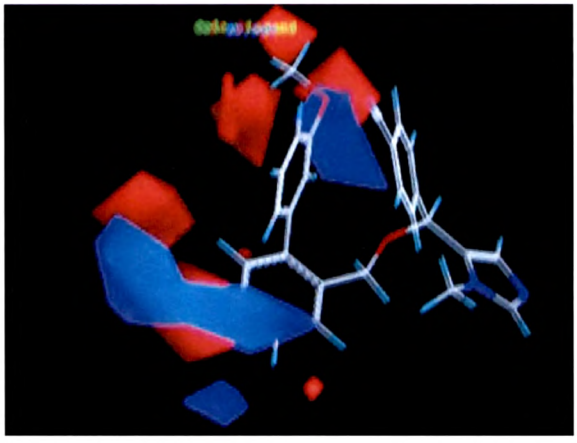

Figure 5.1.5 CoMFA standard deviation coefficient electrostatic contour plots with compound **7**; blue contours indicate regions where positively charged groups increase activity, where red contours indicate regions where negative charge increases activity.

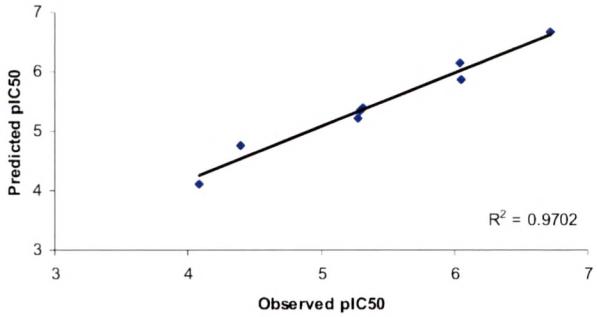

Figure 5.1.6 Graphs of actual *versus* predicted pIC50 of test set molecules obtained from CoMFA model 4.

The most critical and important part of the QSAR model development is the model validation, where the internal predictive power of model and its ability to reproduce biological activities of untested compounds is to be established. This essentially depends on the orientation of ligands and selection of training/test set molecules. The alignment defines the putative pharmacophore for the ligand series and the predictive power of the QSAR models reveals the significance of alignment in the 3D-QSAR model development. The ligand molecules were aligned onto a template structure (compound **7**) employing four different alignment rules **(Figure 5.1.1)** and all

alignments except atom-based alignment III, exhibited statistically significant correlative models with an average to good predictivity, supporting our choice of atoms/centroids for superimposition. The variations in predictivity from the different alignment rules employed in the present study may be due to the rigidity of ligands in the test set as a slight change in their orientations leads to the placement of functional groups in unfavorable regions, supporting the exact superimposition of ligand molecules on the template structure a essential feature for good predictions in 3D-QSAR/CoMFA studies.

CoMFA model (Model 4) generated from alignment IV, which exhibited good internal and maximum external predictivity, was used in the analysis of CoMFA contours **(Figures 5.1.4 and 5.1.5)**. The actual and predicted activities of training and test set of compounds are given in **Tables 5.1.4 and 5.1.5**, respectively.

Table 5.1.4 Actual and predicted biological activities and residuals of the training set compounds by the CoMFA Model 4

C.N	FTase inhibition actual activity [a]	CoMFA-predicted activity	Residuals
1	5.05	5.11	-0.06
2	6.09	5.94	0.15
3	5.95	6.01	-0.06
4	5.88	5.87	0.01
5	6.02	5.92	0.10
6	6.06	6.08	-0.02
7	6.45	6.42	0.03
8	6.06	6.10	-0.04
9	5.95	6.00	-0.05
10	6.16	6.17	-0.01
11	6.01	6.03	-0.02
12	5.92	6.00	-0.08
13	6.07	6.06	0.01
14	5.95	6.10	-0.15
15	6.00	5.98	0.02
16	5.95	5.93	0.02
17	4.45	4.52	-0.07

18	4.95	5.01	-0.06
19	4.88	4.72	0.16
20	5.79	5.29	0.50
21	5.69	5.60	0.09
22	6.01	6.02	-0.01
23	6.35	6.38	-0.03
24	6.11	6.06	0.05
25	5.95	5.98	-0.03
26	5.69	5.82	-0.13
27	5.79	5.74	0.05
28	5.39	5.50	-0.11
29	4.82	4.90	-0.08
30	6.00	5.98	0.02
31	5.58	5.71	-0.13
32	6.21	6.23	-0.02
33	5.65	5.62	0.03
34	6.12	6.21	-0.09

[a] Farnesyltransferase inhibition activity is expressed as log ($1/IC_{50}$)

Table 5.1.5 Actual and predicted biological activities and residuals of the test set compounds by the CoMFA model (Model 4)

C.N	FTase inhibition actual activity [a]	CoMFA-predicted activity	Residuals
35	5.31	5.40	-0.09
36	6.04	6.15	-0.11
37	5.28	5.22	0.06
38	6.72	6.68	0.04
39	4.39	4.76	-0.27
40	4.08	4.11	-0.03
41	6.05	5.86	0.19
42	5.30	5.35	-0.05

[a] Farnesyltransferase inhibition activity is expressed as log ($1/IC_{50}$)

Significant green contours surrounding ring B and the aryl group attached to ring A represent favored steric area to increase inhibition against farnesyltransferase. This is the reason why compounds **5** (napthyl), **8** (3,4-OCH_2O-Ph), **10** (3-OEt-Ph) and **38** (3-CH_2OCH_3-Ph) have shown enhanced farnesyltransferase inhibitory activity. A yellow

contour in the vicinity of cyano group attached to ring A suggests that bulkier substituents on ring A (especially para and meta position which are close to the sterically unfavorable yellow region) are detrimental for FTase inhibitory activity. This is the reason why compounds **17** ($R=SO_2Me$) and **18** ($R=NHCOCH_2OMe$) exhibit poor inhibitory activities than compounds **2** and **3** having chlorine at R position and compounds (**4-15**) which have cyano group at R position.

Significant blue and red contours **(Figure 5.1.5)** surrounding ring A and aryl group attached to ring A represent regions where positively charged and negatively charged substituents favor the farnesyltransferase inhibitory activity. The red contour close to ring A clearly justifies the need of having electronegative substituents (as in compounds where R=Cl or CN) at its para position as observed in most of the compounds. Hence, Compound **39** which has NH_2 group at para position show decreased activity. The substitution pattern on the aryl group is important for enzymatic activity[6]. Red contours are observed in the vicinity of meta position of the aryl group indicating the need of electronegative substituents. Hence, compound **2** and **15** having chlorine and fluorine at meta position, respectively are more potent than **35** which has chlorine at para position (4-Cl-Ph).

A 3D CoMFA model was developed for benzonitrile derivatives as farnesyltransferase inhibitors. As CoMFA is alignment sensitive four different alignment rules were employed in which alignment IV (atom and shape-based RMS fit) yielded statistically significant results. The CoMFA contour maps clearly signify the importance of steric and electrostatic parameters in governing the farnesyltransferase inhibitory activity. A good correlation (r^2 0.9702) could be obtained between the actual and predicted activities of the test set compounds which reflects the predictive power of the model. Further, this model can be used to design potent and selective farnesyltransferase inhibitors belonging to this benzonitrile series.

5.2 Understanding the Antitumor Activity of Novel Tricyclicpiperazinyl Derivatives as Farnesyltransferase Inhibitors using CoMFA and CoMSIA.

5.2.1 Experimental

5.2.1.1 Data set and alignment rule

One hundred and twenty six molecules selected for the present study were taken from the published work by Mallams et al[2]. It is imperative to evaluate the predictivity of the generated 3D-QSAR models. Selection of the training set and test set molecules was done by considering the fact that test set molecules represent a range of biological activity similar to that of the training set. Thus, the test set was the true representative of the training set. The structures of the training and test set molecules are given in **Tables 5.2.1 and 5.2.2,** respectively.

Table 5.2.1 Structures and antitumor activity of compounds used in training set.

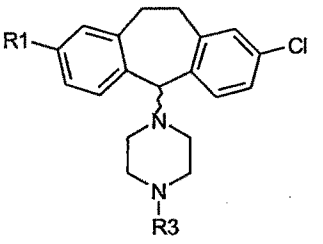

Structure A R1=H
Structure F R1=Br

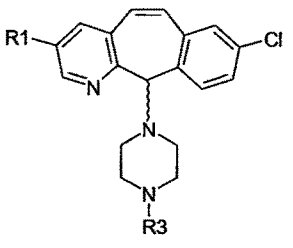

Structure E R1 = H
Structure I R1 = Br

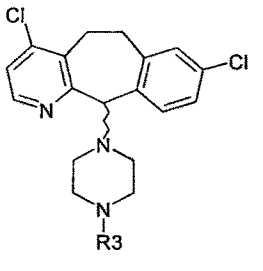

Structure J R3 = H

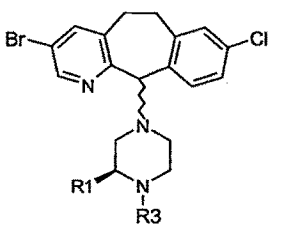

Structure K; R1-n.Bu
Structure L; R1-MeO(CH2)2

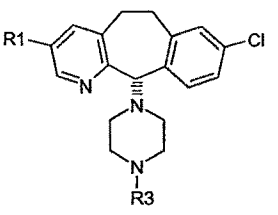

S(-)

Structure C R1 = H
Structure H R1 = Br

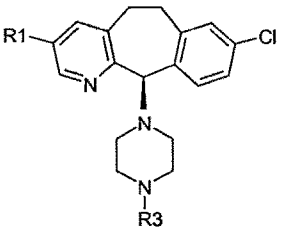

R(+)

Structure G R1 = Br

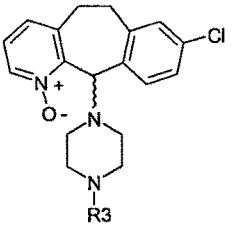

Structure D

C.N	Structure	R_3	pIC50
1	A	-H	4.51
2	A	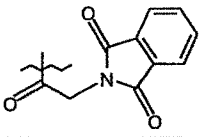	6.08
3	A	$-COCH_2NHBoc$	5.31
4	A	$-COCH_2NHCOCH(SH)CH_3$	5.55
5	A	$-COCH(C_6H_5)_2$	5.60
7	A	$-COCH_2C_6H_4$-4-Br	5.61
8	A	$-COCH_2C_6H_4$-4-NMe_2	4.69
9	A	$-COC_6H_4$-4-NMe_2	6.79
10	A	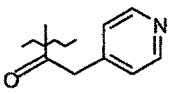	7.92
11	F	-,,-	6.85
12	C	-,,-	6.27
13	A	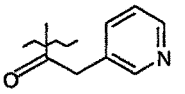	6.76
14	F	-,,-	6.04
15	C	-,,-	6.05
16	D	-,,-	6.44
17	E	-,,-	5.75
18	J	-,,-	6.07

19	A	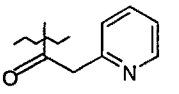	5.30
21	A	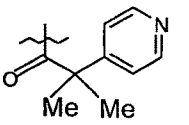	5.74
22	A	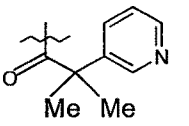	5.93
23	F	-,,-	6.39
24	A	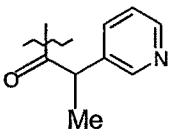	5.42
26	F	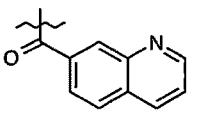	5.34
27	A	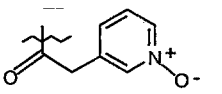	6.13
28	F	-,,-	7.32
30	D	-,,-	6.30
31	E	-,,-	6.48
32	A	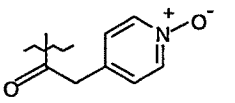	5.90
33	F	-,,-	5.65
34	C	-,,-	6.40
36	J	-,,-	5.90
38	L	-,,-	4.87

39	A	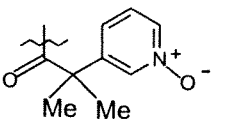	5.36
41	A	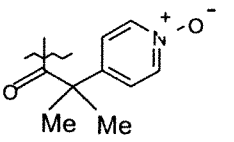	5.16
42	F	-,,,-	4.99
43	A	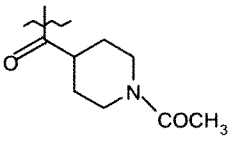	5.85
44	C	-,,,-	6.19
45	A	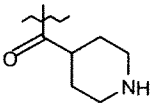	5.86
46	A	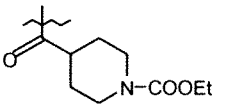	6.34
47	A	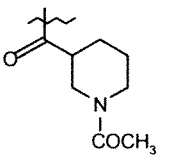	6.06
48	A	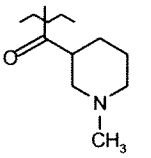	5.79
49	A	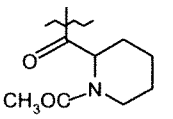	5.13
50	A	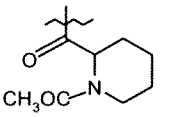	5.90
52	C	-,,,-	7.14
54	E	-,,,-	7.10

55	J	-"-	7.08
56	A	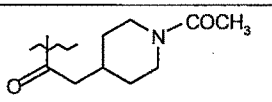	7.16
58	C	-"-	6.46
59	A	-"-	5.88
60	F	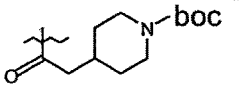	6.08
61	A	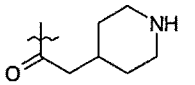	7.31
62	F	-"-	7.31
63	G	-"-	7.34
64	I	-"-	7.56
65	L	-"-	7.03
66	F	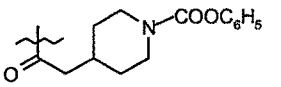	5.97
67	A	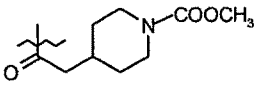	6.03
69	A	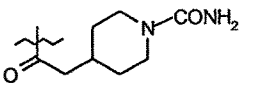	6.05
70	F	-"-	6.00
71	H	-"-	6.96
72	I	-"-	5.60
73	K	-"-	5.60
74	L	-"-	5.95
75	A	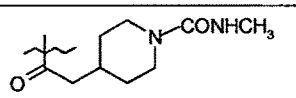	6.98

77	A	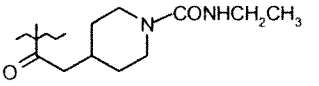	6.63
78	A	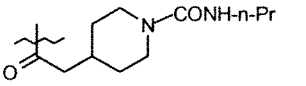	5.92
80	A	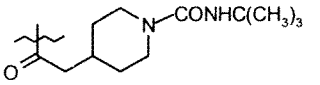	7.00
81	F	-,,,-	6.22
83	A	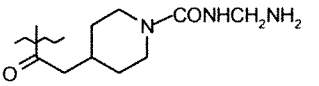	5.77
84	A	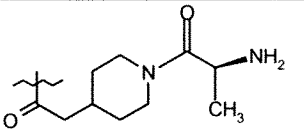	5.15
85	A	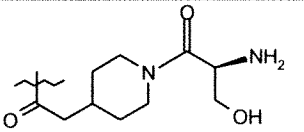	5.15
86	F	-,,,-	5.85
88	F	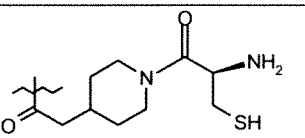	6.30
89	A	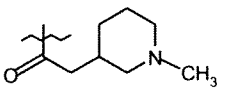	6.08
90	F	-,,,-	5.50
91	C	-,,,-	6.50
92	E	-,,,-	5.67
96	A	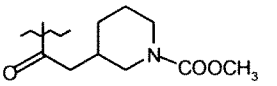	6.05
98	A	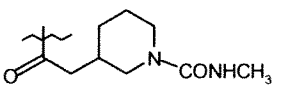	5.00
99	F	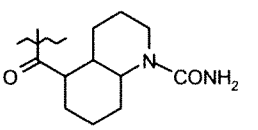	5.75

101	A	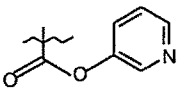	5.96
102	C	-,,-	6.04
103	A	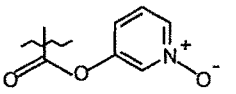	5.87
105	F	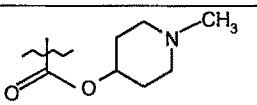	6.67
106	A	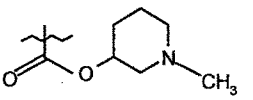	6.33
108	E	-$COOC_6H_5$	5.33
109	A	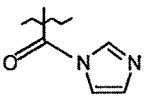	6.02
110	F	-$CONHCH_2C_6H_5$	6.67
111	A	-$CONHC_6H_5$	5.65
112	A	-,,-	6.61
113	A	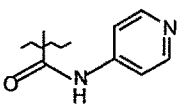	7.38
114	A	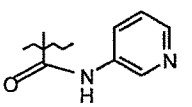	6.18
115	F	-,,-	7.26
116	C	-,,-	6.33
117	A	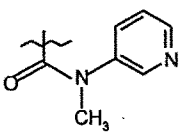	5.33
118	A	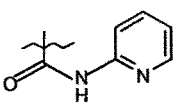	6.02
120	F	-,,-	6.67

121	A	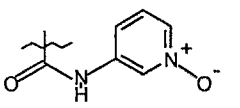	5.65
122	F	-,,-	6.61
124	F	-,,-	7.38
125	A	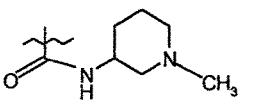	6.18
126	F	-,,-	7.26

Table 5.2.2 Structures and antitumor activity of compounds used in test set.

C.N	Structure	R_3	pIC_{50}
6	A	$-COCH_2C_6H_5$	5.56
20	A	$-COC(CH_3)_2C_6H_5$	5.48
25	A	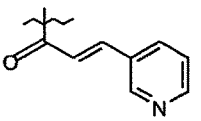	5.58
29	C	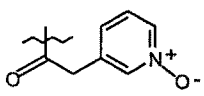	5.63
35	H	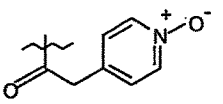	7.63
37	K	-,,-	6.22
40	F	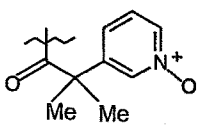	6.42
51	F	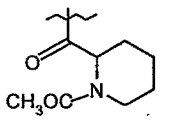	6.92
53	H	-,,-	7.30

57	F	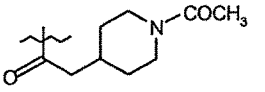	7.00
68	A	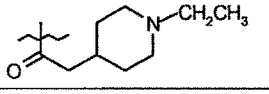	5.89
76	F	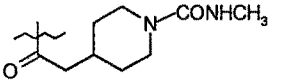	7.30
79	F	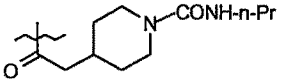	7.00
82	A	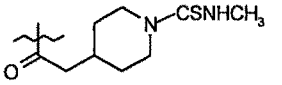	6.05
87	A	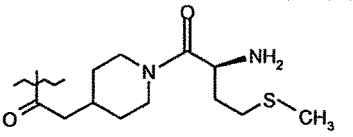	5.72
93	A	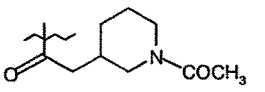	5.50
94	A	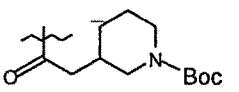	4.91
95	A	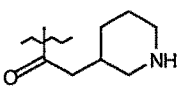	5.95
97	A	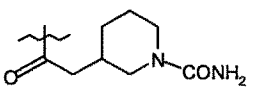	5.75
100	A	-$COOC_6H_5$	6.09
104	F	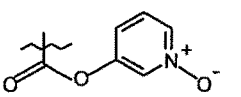	6.55
107	F	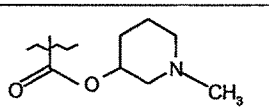	6.52
119	A	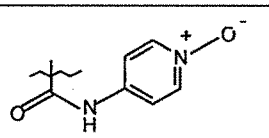	5.74
123	A	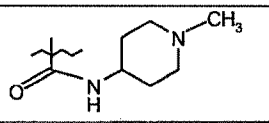	6.32

Alignment rule

The most active and pharmacokinetically stable compound **35** was used as a template for superimposition, assuming that its conformation represents the most bioactive conformation of the tricyclicpiperazinyl derivatives at the enzyme active site. The common fragment shown in **Figure 5.2.1** was selected for DATABASE ALIGNMENT method in SYBYL. The aligned compounds are shown in **Figure 5.2.2**.

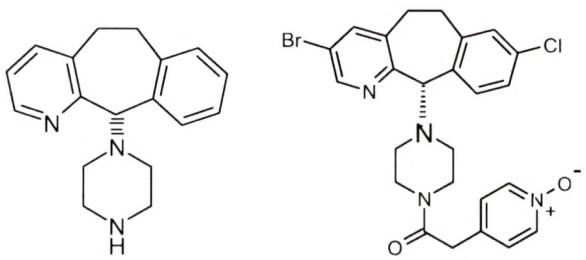

Figure 5.2.1 Common fragment used for alignment and template molecule (compound **35**)

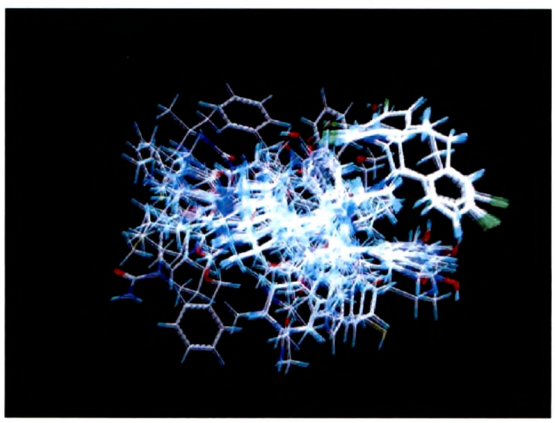

Figure 5.2.2 Alignment of training set of molecules

5.2.2 Results and discussion

One hundred and twenty six tricyclicpiperazinyl derivatives **(Table 5.2.1 and 5.2.2)** were used for the study. Alignment rule employed and the superimposition of all the derivatives are depicted in **Figures 5.2.1 and 5.2.2,** respectively.

5.2.1.1 CoMFA and CoMSIA analyses

The results of CoMFA and CoMSIA studies are summarized in **Tables 5.2.3** and **5.2.4,** respectively. All the analyses reveal comparable cross-validated r^2 values. Analysis 'A' **(Table 5.2.3)** yielded a correlation with an r^2_{cv} of 0.399 (eight principal components) and a conventional r^2 of 0.823. This model displayed poor external predictivity with r^2_{pred} 0.275. Thus, in order to increase the predictive power of the derived model, further experiments were performed. Based on the results of QSAR studies from PLS analysis nine molecules (compounds **7, 15, 17, 23, 38, 44, 45, 60** and **111**) of the training set with high residual values were omitted. Analysis 'B' **(Table 5.2.3)** shows the CoMFA results obtained using the training set of 93 compounds having better confidence level in statistical significance. Analysis B showed improved cross-validated r^2 of 0.550, conventional r^2 of 0.969, F value of 121.990, bootstrapped r^2 of 0.947 and predictive r^2 of 0.543. The steric and electrostatic contributions were found to be 46.2 % and 53.8 %, respectively. The higher contribution of electrostatic fields indicates that the electrostatic interactions of the molecule with the receptor could be an important factor for antitumor activity.

CoMSIA analysis was performed using steric, electrostatic, hydrophobic and hydrogen bond donor and hydrogen bond acceptor fields. Presently CoMSIA offers five different fields. 3D-QSAR models can be generated using the above fields in different combinations. The results of CoMSIA analyses are summarized in **Table 5.2.4.** The CoMSIA models showed considerable correlative and predictive properties. In most of the models, hydrophobic field was a common factor indicating the importance of lipophilicity for the present series of molecules.

The model generated using steric, electrostatic and hydrophobic descriptors has higher r^2_{cv} and comparable r^2_{pred} than rest of the models but has higher standard error of estimate and standard error of prediction.

Table 5.2.3 Summary of CoMFA analysis

Statistical parameters	CoMFA (Analysis - A)	CoMFA (Analysis - B)
r^2_{cv}	0.399	0.550
SEP	0.350	0.480
N	8	6
r^2	0.823	0.909
SEE	0.340	0.215
F - value	83.045	121.990
Prob. of $r^2 = 0$	0.0	0.0
r^2_{pred}	0.375	0.543
r^2_{bs}	0.880	0.947
SD	0.087	0.011
Contributions (fraction)		
Steric	0.450	0.462
Electrostatic	0.550	0.538

Incorporation of all the fields resulted in the reduction of r^2_{cv} and r^2_{pred}. To check whether the addition of hydrogen bond donor or acceptor descriptors affected the model, each descriptor was considered along with steric, electrostatic and hydrophobic descriptors for generating the model.

It was observed that inclusion of hydrogen bond donor descriptor caused reduction in r^2_{cv} (0.580). Whereas, the addition of hydrogen bond acceptor caused increase in the r^2_{cv} (0.611) and also the predictive power (r^2_{pred}) of the model. This indicates the importance of hydrogen bond acceptor functional group for the biological activity. Finally the combination of steric, electrostatic, hydrophobic and hydrogen bond acceptor was selected as the best model on the basis of presence of proper (a) statistical terms and (b) descriptors to explain observed biological activity.

Table 5.2.4 Summary of CoMSIA analysis

Molecular parameters	Statistical parameters								
	r^2_{cv}	SEP	N	r^2	SEE	F	r^2_{bs}	SD	r^2_{pred}
H[a]	0.475	0.503	2	0.925	0.199	96.355	0.961	0.009	0.383
D[b]	0.140	0.653	4	0.619	0.447	14.395	0.676	0.057	0.108
A[c]	-0.161	0.744	1	0.629	0.441	15.043	0.754	0.058	-0.202
D+A	-0.039	0.717	4	0.798	0.323	40.457	0.868	0.023	0.123
H+D	0.574	0.459	4	0.900	0.227	92.315	0.936	0.016	0.282
H+A	0.454	0.520	4	0.934	0.185	145.364	0.962	0.010	0.667
H+D+A	0.508	0.493	4	0.939	0.177	158.138	0.965	0.008	0.541
H+S[d]+E[e]	0.631	0.430	6	0.953	0.156	208.365	0.973	0.005	0.529
S+E+D	0.451	0.520	6	0.957	0.149	230.015	0.970	0.006	-0.007
S+E+A	0.355	0.577	7	0.944	0.169	174.930	0.960	0.012	0.544
S+E+D+A	0.399	0.557	7	0.958	0.148	233.327	0.965	0.005	0.554
S+E+D+A+H	0.535	0.493	8	0.980	0.101	445.103	0.987	0.001	0.634
S+E+A+H#	**0.611**	**0.451**	**6**	**0.971**	**0.123**	**299.318**	**0.986**	**0.004**	**0.663**
S+E+D+H	0.580	0.469	8	0.980	0.101	445.103	0.991	0.006	0.621
ALL	0.466	0.514	4	0.976	0.113	354.709	0.984	0.005	0.401

a- Hydrophobic field; b- Hydrogen bond donor field; c- Hydrogen bond acceptor field
d- Steric field; e- Electrostatic field; #- Best model for CoMSIA

The real test for the model predictiveness is to predict the activity of compounds, which were not used in the model generation. To check the external predictivity of the model, we used the test set, which comprised of 24 compounds. Both the CoMFA and CoMSIA models exhibited a good predictiveness on these compounds.

The observed and calculated activity values along with residuals for training and test set molecules are given in **Tables 5.2.5 and 5.2.6**, respectively. The plots of calculated vs observed activity values for training set molecules and predicted *versus* observed activity values for the test set molecules are shown in **Figures 5.2.3** and **5.2.4**, respectively.

Table 5.2.5 Actual, predicted inhibitory activities (pIC_{50}) and residuals of the training set molecules (Using analysis - B of CoMFA and best model from CoMSIA analysis).

C.N	Actual pIC_{50}	Predicted pIC_{50}		Residuals	
		CoMFA	CoMSIA	CoMFA	CoMSIA
1	4.51	4.42	4.50	0.09	0.01
2	6.08	6.32	5.70	-0.24	0.38
3	5.31	5.25	5.52	0.06	-0.21
4	5.55	5.60	5.605	-0.05	-0.07
5	5.60	5.52	5.44	0.08	0.16
8	5.61	5.66	5.64	-0.05	-0.03
9	4.69	4.69	5.01	0.00	-0.32
10	6.79	6.80	6.94	-0.01	-0.14
11	7.92	7.36	7.33	0.56	0.53
12	6.85	6.91	6.55	-0.06	0.30
13	6.27	6.08	6.00	0.19	0.27
14	6.76	6.92	6.927	-0.16	-0.16
16	6.04	6.10	5.97	-0.06	0.07
18	6.05	6.10	6.09	-0.05	-0.04
19	6.44	6.31	6.04	0.11	0.40
21	5.75	5.56	5.75	0.19	0.00
22	6.07	5.53	6.10	0.54	-0.03
24	5.30	5.92	5.21	-0.62	0.09
26	5.74	5.93	5.96	-0.19	-0.22
27	5.93	5.84	5.64	0.09	0.31
28	6.39	6.58	6.60	-0.19	-0.21
30	5.42	5.51	5.49	-0.09	-0.07
31	5.34	5.38	5.40	-0.04	-0.06
32	6.13	6.46	6.28	-0.33	-0.15
33	7.32	7.08	7.20	0.24	0.12
34	6.30	6.21	6.46	0.09	-0.16
36	6.48	6.39	6.42	0.09	0.06
39	5.90	5.92	5.98	-0.02	-0.08
41	5.65	5.71	5.51	-0.06	0.14
42	6.40	6.67	6.47	-0.27	-0.07
43	5.90	5.58	5.68	0.32	0.22
46	4.87	5.00	4.89	-0.13	-0.02
47	5.36	5.20	5.24	0.16	0.12
48	5.16	5.26	5.38	-0.10	-0.22
49	4.99	5.20	5.31	-0.21	-0.32

50	5.85	5.94	5.90	-0.09	-0.05
52	6.19	6.18	6.02	0.01	0.17
54	5.86	5.80	5.82	0.06	0.04
55	6.34	6.25	6.29	0.09	0.05
56	6.06	6.13	5.92	-0.07	-0.86
58	5.79	6.28	6.00	-0.49	-0.21
59	5.13	5.12	5.35	0.01	-0.22
61	5.90	6.00	5.97	-0.10	-0.07
62	7.14	7.11	7.23	0.03	-0.09
63	7.10	6.95	7.34	0.15	-0.24
64	7.08	7.00	7.18	0.08	-0.10
65	7.16	7.38	6.45	-0.22	0.71
66	6.46	6.62	6.54	-0.16	-0.08
67	5.88	5.83	5.66	0.05	0.20
69	6.08	6.24	6.15	-0.16	-0.07
70	7.31	7.21	7.42	0.10	-0.11
71	7.31	6.73	7.18	0.58	0.13
72	7.34	7.11	7.21	0.23	0.13
73	7.56	7.72	7.41	-0.16	0.15
74	7.03	6.98	7.00	0.05	0.03
75	5.97	6.11	5.97	-0.14	0.00
77	6.03	6.09	5.96	-0.06	0.07
78	6.05	6.10	5.96	-0.05	0.09
80	6.00	5.80	5.91	0.20	0.09
81	6.96	6.80	7.03	0.16	-0.07
83	5.60	5.66	5.67	-0.06	-0.07
84	5.60	5.64	5.63	-0.04	-0.03
85	5.95	5.63	5.78	0.32	0.17
86	6.98	6.94	6.94	0.037	0.04
88	6.63	6.82	6.55	-0.19	0.08
89	5.92	5.95	5.94	-0.03	-0.02
90	7.00	6.99	6.78	0.01	0.22
91	6.22	6.20	6.09	0.02	0.13
92	5.77	6.31	6.10	-0.54	-0.33
96	5.15	5.32	5.47	-0.17	-0.32
98	5.15	5.12	4.98	0.03	0.17
99	5.85	6.01	5.77	-0.16	0.08
101	6.30	6.08	5.95	0.22	0.35
102	6.08	6.16	6.13	-0.08	-0.05
103	5.50	5.57	5.63	-0.07	-0.13
105	6.50	6.47	6.46	0.13	0.04
106	5.67	5.18	5.61	0.49	0.06

108	6.05	5.99	6.00	0.06	0.05
109	5.00	4.83	4.73	0.17	0.27
110	5.75	5.78	5.70	0.03	0.05
112	5.96	6.06	5.99	-0.10	-0.03
113	6.04	6.16	6.05	-0.12	-0.01
114	5.87	5.99	6.02	-0.12	-0.15
115	6.67	6.59	6.62	0.08	0.05
116	6.33	6.34	6.39	-0.01	-0.06
117	5.33	5.45	5.49	-0.12	-0.16
118	6.02	5.68	5.82	0.34	0.20
120	6.67	6.53	6.75	0.14	-0.08
121	5.65	5.77	5.78	-0.12	-0.13
122	6.61	6.58	6.68	0.03	-0.07
124	7.38	7.12	7.41	0.26	-0.03
125	6.18	6.18	6.28	0.00	-0.10
126	7.26	7.03	7.15	0.23	0.11

Table 5.2.6 Actual, predicted inhibitory activities (pIC_{50}) and residuals of the test set molecules (Using analysis – B of CoMFA and best model from CoMSIA analysis)

C.N	Actual pIC_{50}	Predicted pIC_{50}		Residuals	
		CoMFA	CoMSIA	CoMFA	CoMSIA
6	5.56	5.68	5.60	-0.12	-0.04
20	5.48	5.69	5.97	-0.21	-0.49
25	5.58	5.30	5.81	0.28	-0.23
29	5.63	6.64	6.66	-1.01	-1.03
35	7.63	6.52	6.70	1.11	-0.93
37	6.22	6.54	7.05	-0.32	-0.83
40	6.42	6.80	6.91	-0.38	-0.49
51	6.92	6.90	6.72	0.02	0.20
53	7.30	6.44	6.36	0.86	0.94
57	7.00	7.01	6.86	-0.01	-0.86
68	5.89	5.81	5.84	0.08	0.05
76	7.30	6.98	7.02	0.32	0.28
79	7.00	6.92	7.04	0.08	-0.04
82	6.05	5.60	5.65	0.45	0.40
87	5.72	5.63	5.57	0.09	0.15
93	5.50	6.28	5.94	-0.78	-0.44
94	4.91	5.97	5.74	-1.06	-0.84

95	5.95	6.03	6.06	-0.08	-0.11
97	5.75	5.67	5.80	0.08	-0.05
100	6.09	5.73	5.97	0.36	-0.12
104	6.55	6.22	6.75	0.30	-0.20
107	6.52	6.24	6.48	0.28	0.04
119	5.74	5.41	5.84	0.33	-0.10
123	6.32	6.15	5.97	0.17	0.35

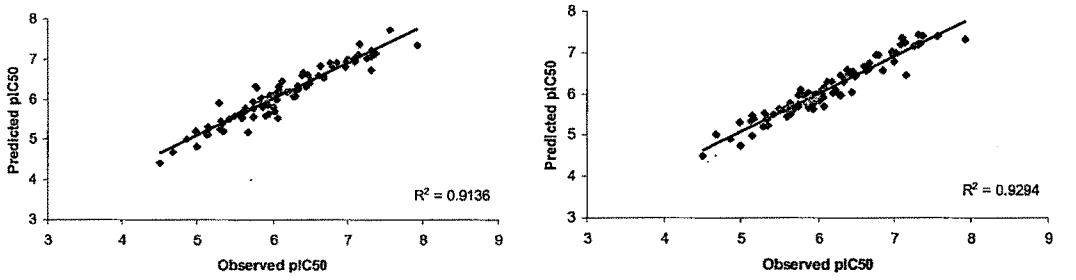

Figure 5.2.3 Calculated *vs* observed activity from **(I)** CoMFA and **(II)** CoMSIA analyses of the training set.

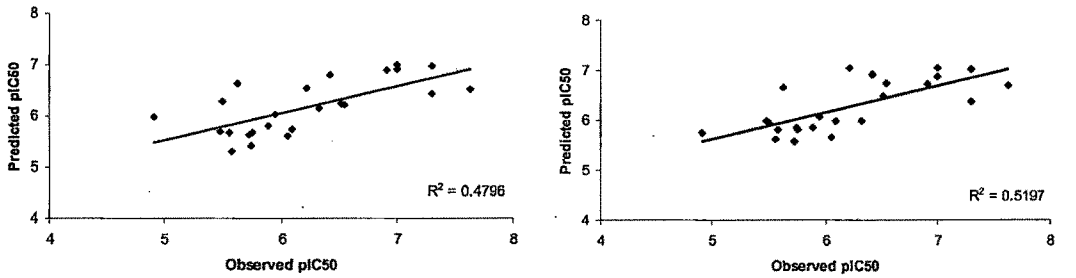

Figure 5.2.4 Observed *vs* predicted activity from (a) CoMFA and (b) CoMSIA analyses of the test set.

5.2.2.2 Graphical interpretation of the results

To visualize the information contents of the derived 3D-QSAR model, CoMFA contour maps were generated by interpolating the products between the 3D-QSAR coefficients

and their associated standard deviations. **Figures 5.2.5** and **5.2.6** indicate the CoMFA steric and electrostatic contour maps, respectively obtained from analysis-B using compound **35** as a reference structure. In this figure, the green contours represent regions of high steric tolerance, while the yellow contours represent regions of low steric bulk tolerance. The increase in positive charge is favored in blue regions while increase in negative charge is favored in red regions.

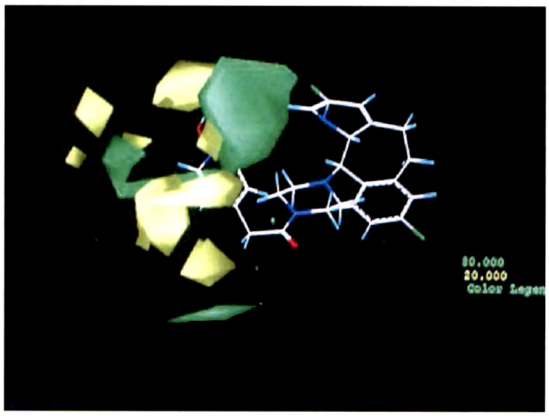

Figure 5.2.5 The CoMFA steric STDEV*COEFF contour plots of active compound **35** from analysis-B. Sterically favored areas (contribution level 80%) are represented by green polyhedra. Sterically disfavored areas (contribution level 20%) are represented by yellow polyhedra.

The steric contours of CoMFA **(Figure 5.2.5)** showed a large green contour enclosing the pyridyl acetyl N-oxide (R_3 substituent) of the template structure. This indicates that bulky R_3 substituents on the piperazine will enhance the farnesyltransferase inhibitory activity. The good inhibitory potency of **70** (IC_{50} 0.049), **71** (IC_{50} 0.048), **72** (IC_{50} 0.045), **73** (IC_{50} 0.027) and **74** (IC_{50} 0.092) are due to orientation of their 4-carboxamidopiperidinylacetamido group towards sterically favored green contour. Compound **1** lacking bulky group at the 4^{th} position of the piperazine was very less active. The steric contours also show yellow contour in the vicinity of the aromatic ring of the R_3 substituent attached to the piperazine. Here, bulky substituents are not tolerated and hence the molecules **4** (IC_{50} 2.78) and **110** (IC_{50} 1.77) exhibit low inhibitory activity.

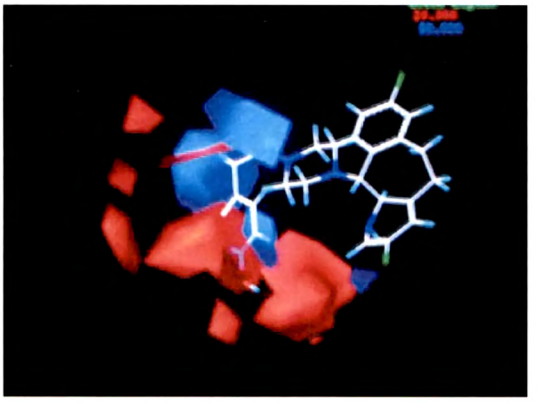

Figure 5.2.6 The CoMFA electrostatic STDEV*COEFF contour plots of active compound **35** from analysis-B. Positively charged favored areas (contribution level 80%) are represented by blue polyhedra. Negatively charged favored areas (contribution level 20%) are represented by red polyhedra.

The electrostatic contours of CoMFA **(Figure 5.2.6)** shows red contour enclosing the pyridine ring of the template molecule where high electron density is expected to increase the activity. Hence, the N-oxide derivatives (**33**, **34**, **36**, **38**, **124**) exhibit good activity where the electronegative oxygen is buried in red contour. This is because N-oxide increases electron density which is favorable for inhibitory activity. The electrostatic contours also show blue polyhedra in the vicinity of piperazine ring where low electron density is expected to increase activity. Compound **7** (IC_{50} 2.04) exhibits low activity as the electronegative bromide group is embedded in the blue contours.

The hydrophobic contours **(Figure 5.2.7)** show presence of a large purple contour surrounding the pyridine ring of the template molecule indicating that hydrophobic substituents are well tolerated in that region.

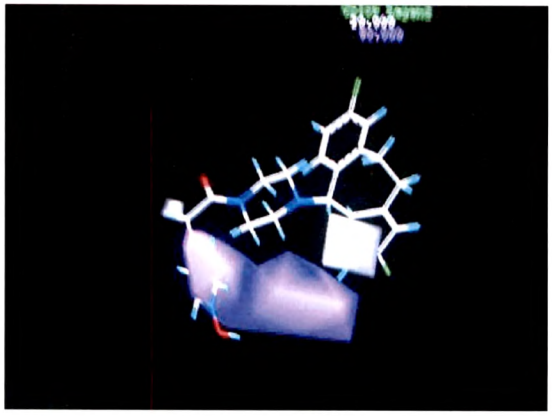

Figure 5.2.7 CoMSIA hydrophobic fields. Purple polyhedra indicate regions where hydrophobic substituents are favored and white plyhedra indicates disfavored regions.

The hydrogen bond acceptor contours **(Figure 5.2.8)** show presence of small magneta contours close to the piperazine ring of the template molecule, where hydrogen bond acceptor substituents will increase the activity. Two cyan contours are seen; one close to the pyridyl nitrogen and one enclosing the aromatic substituent attached to piperazine, indicating the regions in space where hydrogen bond acceptor groups are not tolerated. The developed CoMFA and CoMSIA models are predictive enough to guide the design of new molecules in the series.

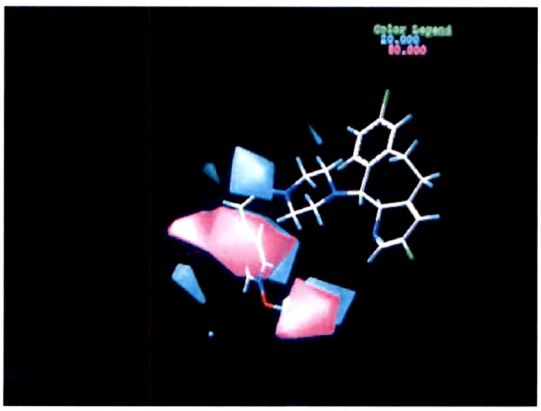

Figure 5.2.8 CoMSIA hydrogen bond acceptor contour plots. Magneta polyhedra indicate regions where hydrogen bond acceptor substituents are favored and cyan plyhedra indicates disfavored regions.

5.2.2.3 CoMFA *versus* CoMSIA

Comparison of the statistical results of the two QSAR analyses is given in **Table 5.2.7.** The cross-validated r^2, conventional r^2, and predictive r^2 are normally accepted as the statistical measures for the quality of QSAR models. Both CoMFA and CoMSIA models exceeded $r^2_{cv} > 0.5$ which indicated stability of the model and reasonable predictability.

Table 5.2.7 Comparison of statistical parameters for two QSAR based techniques

Technique	r^2_{cv}	SEP	N	r^2	SEE	F	r^2_{bs}	SD	r^2_{pred}
CoMFA	0.550	0.480	6	0.969	0.215	121.990	0.947	0.011	0.543
CoMSIA	0.611	0.451	6	0.971	0.123	299.318	0.986	0.004	0.663

CoMSIA showed higher cross-validated r^2 value of 0.611 than 0.550 for CoMFA. The standard error of estimate was also less (0.123) than CoMFA (0.215). Finally the predictive power (r^2_{pred}) value was also on a higher side for CoMSIA than CoMFA.

5.3 Insights into the structural requirements of farnesyltransferase inhibitor benzonitriles as potential anti-tumor agents based on 3D QSAR CoMFA and CoMSIA models

5.3.1 Experimental

5.3.1.1 Data set and alignment rule

Data set for analysis

The training and test set used in the computational studies comprising of molecules belonging to three different benzonitrile classes are reported as FTase inhibitors. The FTase inhibitory data has been collected from the literature[3-5]. The structures and biological activity data of training and test set molecules are described in **Tables 5.3.1-5.3.3.**

Table 5.3.1 Structures and biological activities of 3-aminopyrrolidinone derivatives[3]

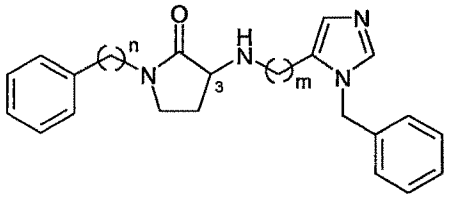

C.N	n	m	Stereo-Chemistry at C-3	FTase inhibition (pIC_{50})		
				Actual	Calculated	
					CoMFA	CoMSIA
1*	0	1	S	7.13	7.82	7.74
2	0	1	R	6.69	6.60	6.92
3	1	1	S	7.53	7.73	7.68
4	1	1	R	7.30	7.25	7.20
5	2	1	S	6.63	6.93	6.68
6#	2	1	R	6.60	7.54	-
7	0	2	S	6.55	6.52	6.24
8	0	2	R	6.92	6.94	6.97
9*	1	2	S	6.56	6.86	6.22

10	1	2	R	6.60	6.56	6.69
11	2	2	S	6.61	6.47	6.61
12	2	2	R	6.42	6.53	6.36

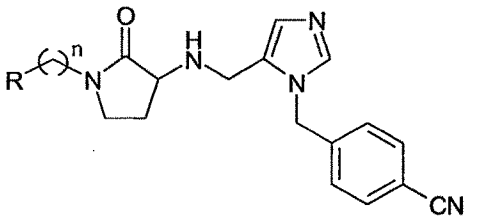

C.N	n	R	FTase inhibition (pIC_{50})		
			Actual	Calculated	
				CoMFA	CoMSIA
13*	0	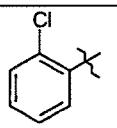	8.82	8.25	7.93
14	0	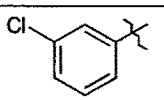	8.08	7.95	7.93
15	0	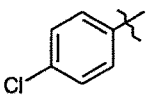	7.68	7.88	7.84
16	1	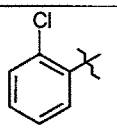	8.28	8.01	8.04
17	1	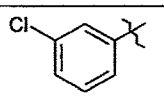	8.72	8.55	8.43
18	1	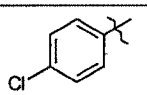	7.60	7.74	7.91
19#	0	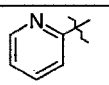	6.43	7.50	-
20	0	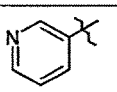	7.07	7.03	6.91
21*	0	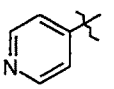	7.37	7.16	6.87

22*	0	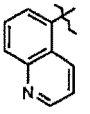	8.00	7.88	7.37

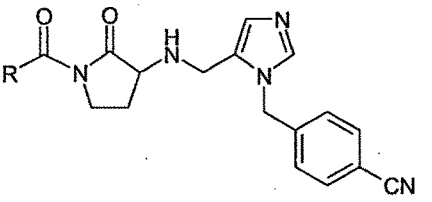

C. N	R	FTase inhibition (pIC_{50})		
		Actual	Calculated	
			CoMFA	CoMSIA
23	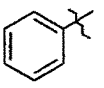	6.96	7.00	7.04
24	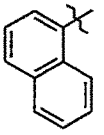	7.96	8.18	7.76
25	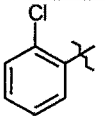	7.19	7.15	7.17
26	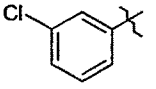	7.57	7.31	7.42
27	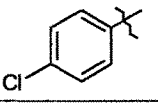	7.05	7.21	7.19
28	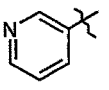	5.70	5.54	5.78
29#	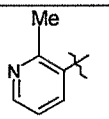	7.00	7.91	-
30	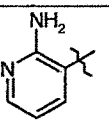	6.01	5.58	6.22

31	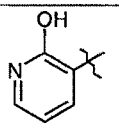	5.17	5.82	6.35
32	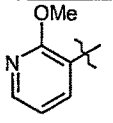	6.82	6.67	6.20
33	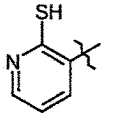	5.54	5.52	6.02
34	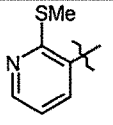	7.08	7.03	7.05
35	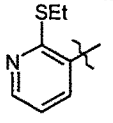	8.32	8.25	8.31
36	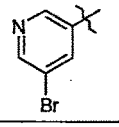	7.37	7.33	7.44

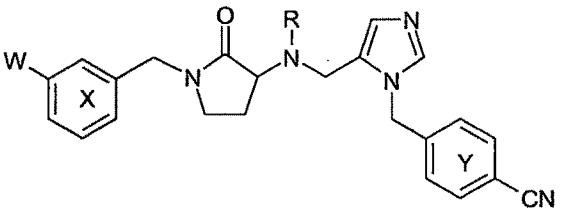

C. N	W	R	FTase inhibition (pIC_{50})		
			Actual	Calculated	
				CoMFA	CoMSIA
37	H	n.Pr	7.23	7.25	7.11
38*	H	n.Bu	7.27	7.30	7.18
39	H	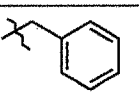	7.17	7.12	7.01
40	H	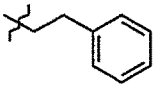	7.29	7.31	7.21

41	H	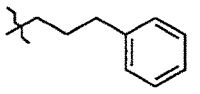	7.82	7.79	7.90
42	H	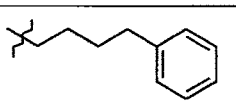	7.38	7.36	7.32
43	H	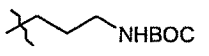	7.74	8.09	8.27
44	H	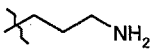	7.77	7.84	7.79
45*	H	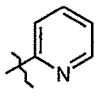	7.28	7.85	7.77
46	Cl	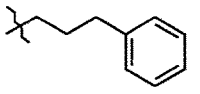	8.60	8.67	8.71
47	Cl	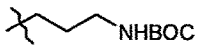	8.89	8.51	8.61
48	Cl	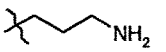	8.12	8.06	8.13
49#	Cl	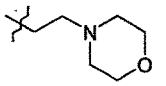	8.22	8.90	-
50#	Cl	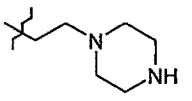	8.21	9.11	-

* Compounds belonging to test set; # outliers

Table 5.3.2 Structures and biological activities of 2-aminonicotinonitriles[4]

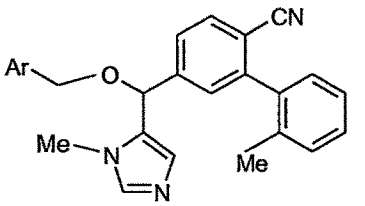

C.N	Ar	FTase inhibition (pIC_{50})		
		Actual	Calculated	
			CoMFA	CoMSIA
51	phenyl	7.07	7.06	7.37
52	*o*-Tolyl	7.26	7.39	7.14
53	*m*-Tolyl	7.21	7.11	7.26
54*	*p*- Tolyl	7.26	7.26	7.21

55	*p*-^{i}Pr-phenyl	7.29	7.26	7.06
56	*p*-^{t}Bu-phenyl	7.06	7.03	6.97
57	*p*-Phenyl-phenyl	7.88	7.87	7.58
58	1-Napthyl	7.76	7.79	7.69
59	8-Quinolyl	7.22	7.23	7.27
60*	*p* -Methoxyphenyl	7.22	7.52	7.90
61	*m* -F_3CO-phenyl	8.08	8.14	7.94
62	*p* -F_3CO-phenyl	7.79	7.74	7.79
63#	*m*-F_3C-phenyl	8.09	9.00	-
64*	*p* -F_3C-phenyl	7.92	7.90	7.91
65	*o* -Cyano-phenyl	7.20	7.17	7.34
66*	*m* -Cyano-phenyl	7.74	7.72	7.56
67	*p* -Cyano-phenyl	8.39	8.37	8.09
68	*o* -Cl-phenyl	7.31	7.32	7.38
69	*m* -Cl-phenyl	7.72	7.57	7.68
70	*p* -Cl-phenyl	7.95	7.80	7.86
71	*m*-Br-phenyl	7.88	7.60	7.73
72	*p* -Br-phenyl	7.92	7.83	7.86
73	*m*-I-phenyl	7.69	7.70	7.77
74	*p* -I-phenyl	7.88	7.93	7.88
75	*o* -NO_2-phenyl	7.48	7.48	7.57
76	*p* -NO_2-phenyl	8.12	8.12	8.31
77*	*m*-CO_2CH_3-phenyl	7.21	7.43	7.52
78#	*p*-CO_2CH_3-phenyl	8.21	8.88	-
79#	*p*-CH_3SO_2-phenyl	7.42	8.00	-
80	3,4-Cl,Cl-phenyl	7.56	7.78	7.65
81	3,5-Cl,Cl-phenyl	7.72	7.70	7.52
82	2,6-Cl,Cl-phenyl	7.09	7.11	6.98
83	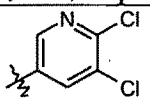	7.82	7.73	7.90
84*	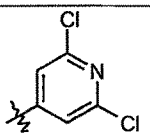	7.88	7.74	7.76
85	*o*-F-phenyl	7.15	7.25	7.46
86	*m*-F-phenyl	7.42	7.56	7.68
87	*p*-F-phenyl	7.49	7.56	7.82
88*	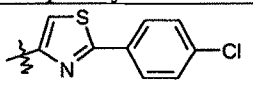	7.53	7.41	7.44

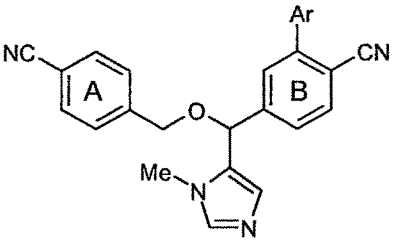

C.N	Ar	FTase inhibition (pIC_{50})		
		Actual	Calculated	
			CoMFA	CoMSIA
89	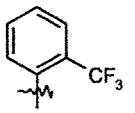	9.09	8.92	8.81
90	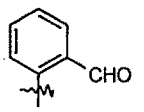	8.72	8.76	8.69
91	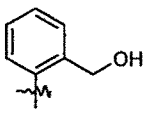	8.25	8.36	8.12
92#	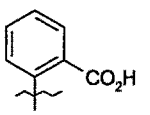	7.85	8.77	-
93#	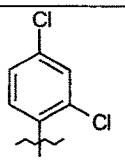	7.32	7.99	-
94	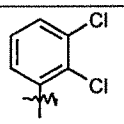	8.82	8.82	8.93
95	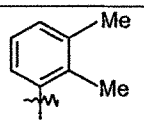	8.67	8.66	8.71
96#	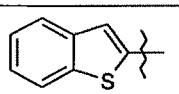	6.79	7.80	-
97	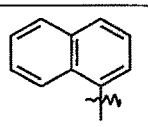	9.69	9.58	9.60

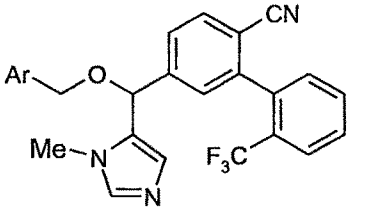

C.N	Ar	FTase inhibition (pIC_{50})		
		Actual	Calculated	
			CoMFA	CoMSIA
98	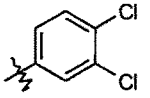	8.76	8.81	8.76
99*	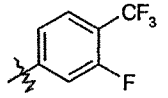	8.21	8.50	8.27
100*	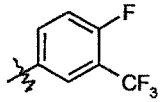	8.38	8.51	8.59
101#	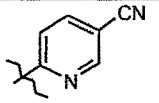	8.56	8.94	-
102*	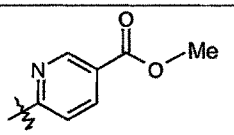	8.04	8.75	8.59

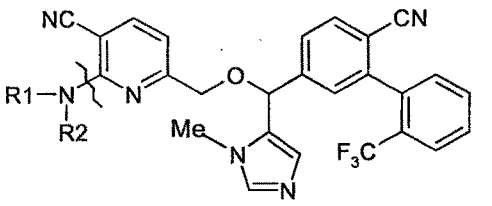

C.N	NR_1R_2	FTase inhibition (pIC_{50})		
		Actual	Calculated	
			CoMFA	CoMSIA
103	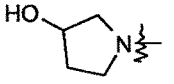	8.45	8.47	8.37

104	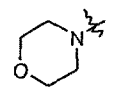	8.88	8.89	8.86
105	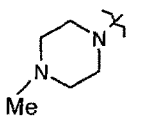	8.92	8.93	8.84
106	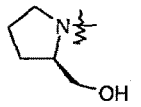	8.69	8.63	8.57
107	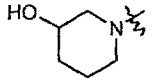	8.88	8.90	8.88
108*	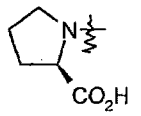	8.44	8.67	8.69
109	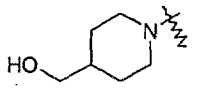	8.74	8.73	8.75
110*	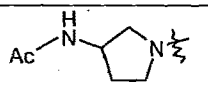	8.76	8.55	8.56
111	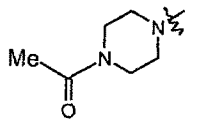	8.58	8.55	8.50
112	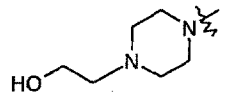	8.88	8.91	8.99
113	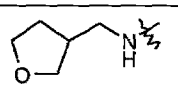	8.11	8.06	8.14
114	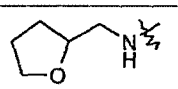	8.17	8.14	8.16
115	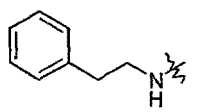	8.04	8.03	7.99
116*	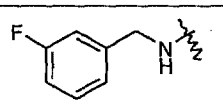	8.00	8.71	7.91

* Compounds belonging to test set; # outliers

Table 5.3.3 Structures and biological activities of 1-aryl-1'-imidazolylmethyl ethers[5]

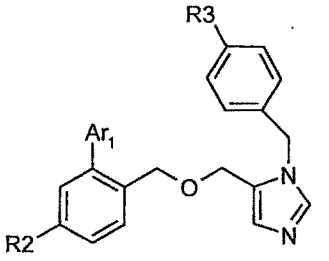

C.N	Ar_1	R_2	R_3	FTase inhibition (pIC_{50})		
				Actual	Calculated	
					CoMFA	CoMSIA
117	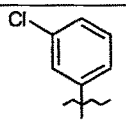	Cl	CN	9.20	9.13	9.13
118	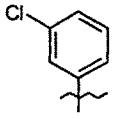	CN	CN	9.43	9.29	9.28
119#	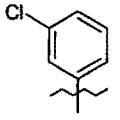	CN	$MeSO_2$	7.01	7.92	-
120	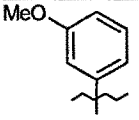	CN	Cl	8.65	8.62	8.69
121	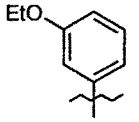	CN	Cl	8.85	8.83	8.76
122	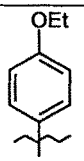	CN	CN	8.92	8.96	9.07
123	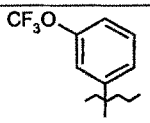	CN	CN	9.30	9.37	9.37
124*	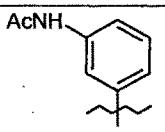	CN	CN	9.18	8.88	8.88

125	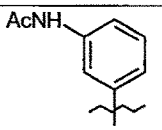	CN	CN	7.88	7.90	7.81
126	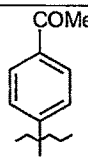	CN	CN	8.88	8.82	8.88
127	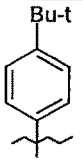	CN	CN	9.35	9.38	9.38
128	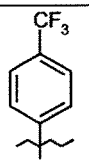	CN	CN	8.36	8.42	8.58
129*	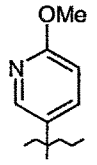	CN	CN	8.11	8.93	8.98
130	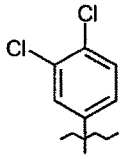	CN	CN	9.43	9.39	9.43
131	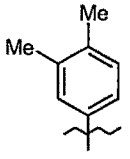	CN	CN	9.22	9.22	9.10
132	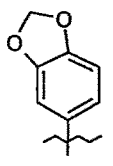	CN	Cl	8.08	8.05	8.02
133	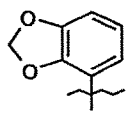	CN	CN	9.09	9.09	9.09
134	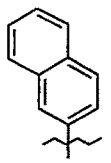	CN	CN	9.03	9.01	9.13

135*	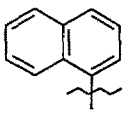	CN	CN	8.88	9.01	9.13

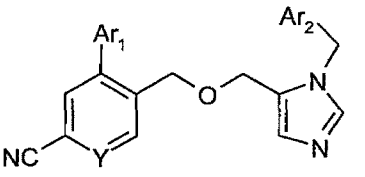

C.N	Ar_1	Y	Ar_2	FTase Inhibition (pIC_{50})		
				Actual	Calculated	
					CoMFA	CoMSIA
136	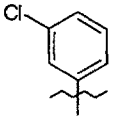	N	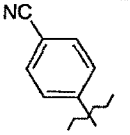	8.36	8.35	8.35
137	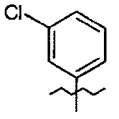	CH	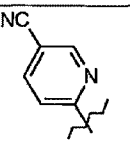	8.76	8.73	8.71
138	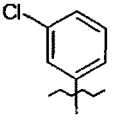	CH	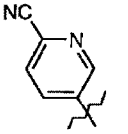	8.52	8.53	8.54
139	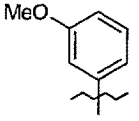	CH	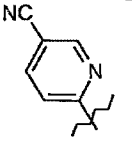	8.35	8.33	8.39
140*	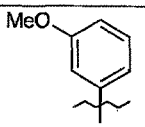	CH	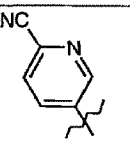	8.82	8.49	8.31
141	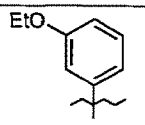	CH	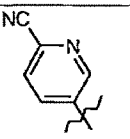	9.23	9.23	9.24
142	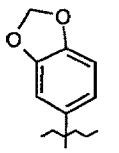	CH	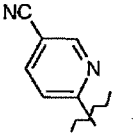	8.32	8.31	8.34

143	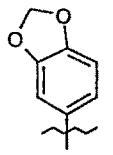	CH	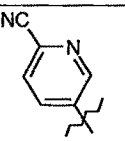	8.52	8.52	8.50

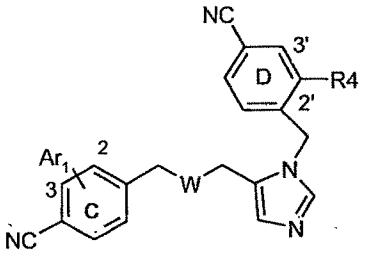

C.N	Ar_1	W	R_4	FTase Inhibition (pIC_{50})		
				Actual	Calculated	
					CoMFA	CoMSIA
144	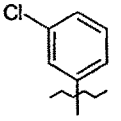	O	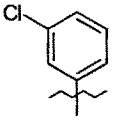	8.00	8.05	8.03
145*	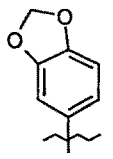	O	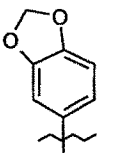	7.46	7.41	7.40
146	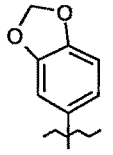	O	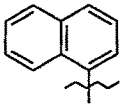	8.16	8.14	8.20
147	H	O	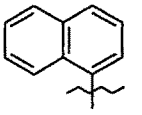	9.01	9.03	8.96
148	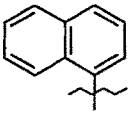	O	H	8.31	8.28	8.27
149	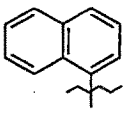	NH	H	8.18	8.16	8.18

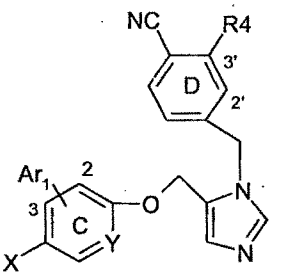

C.N	Ar_1	X	Y	R_4	FTase Inhibition (pIC_{50})		
					Actual	Calculated	
						CoMFA	CoMSIA
150#	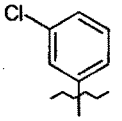	Cl	CH	H	8.39	7.20	-
151	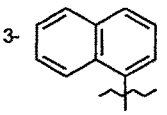	CN	CH	H	9.42	9.45	9.32
152	H	CN	CH	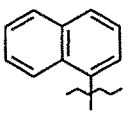	9.49	9.50	9.55
153	H	CN	N	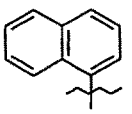	9.04	9.03	9.01

* Compounds belonging to test set; # outliers

Alignment rule:

Atom based alignment approach has been employed in order to calculate the CoMFA and CoMSIA interaction energies **(Figure 5.3.1)** for all the three series of compounds.

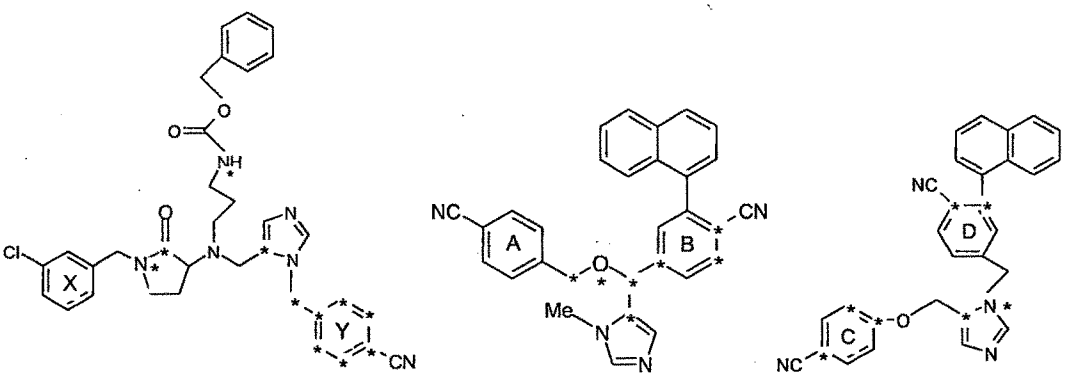

47 (Alignment I) **97 (Alignment II)** **152 (Alignment III)**

Figure 5.3.1 Template structures and atoms used in the rms alignments

5.3.2 Results and discussion

Molecules belonging to three different benzonitrile classes were used for 3D QSAR studies **(Tables 5.3.1-5.3.3)**. The alignment rule employed is depicted in **Figure 5.3.1.** Different alignment rules were tried (for all the three classes of compounds) but only the alignment rule that yielded statistically significant and predictive models are discussed here.

The 3D-QSAR models using CoMFA and CoMSIA methodologies were derived for the three different benzonitrile classes. The structures and biological activity data of the molecules are described in **Tables 5.3.1-5.3.3.** The *in vitro* FTase inhibitory activity values pIC_{50} were used as dependant variable and CoMFA/CoMSIA fields as independent variables in the study. The low energy conformer obtained from MULTISEARCH option in SYBYL was used in the molecular alignment method

performed by atom-based rms fitting. As CoMFA is alignment sensitive, different alignment rules were employed but only the alignments yielding best results have been discussed. One of the major obstacles in the 3D-QSAR studies lies with the 'congeners', which misfit the final equation and were termed as outliers. Removal of outliers increased the statistical quality and predictive power of the models. The reasons for the poor prediction may be their structural uniqueness or the insignificant mathematical value in defining the biological activity. Exceptions were also observed wherein experimentally observed parameters might be better than the calculated or vice versa; however their inclusion in 3D QSAR studies at the cost of lower r^2 could be more confusing than helpful.

The 3D-QSAR models were generated from training set molecules and validated by predicting activity of test set molecules. All cross-validated results were analyzed by considering the fact that the value of r^2_{cv} above 0.3 indicates that the probability of chance correlation is less than 5 %. The results of PLS analysis from CoMFA studies are summarized in **Table 5.3.4** and that from CoMSIA studies in **Tables 5.3.5-5.3.7.** Comparison of the statistical results of the best models obtained by CoMFA and CoMSIA are summarized in **Table 5.3.8.**

5.3.2.1 CoMFA models

3-Aminopyrrolidinone derivatives

3D QSAR models for 3-aminopyrrolidinones reported by Bell et al[3] as selective FTase inhibitors **(Table 5.3.1)** were initially developed using 41 training set molecules and validated by predicting activity for nine test set molecules (Analysis A). The CoMFA model developed from steric and electrostatic fields yielded cross-validated r^2 (r^2_{cv}) 0.526 at seventh component, non-cross-validated r^2 (r^2_{ncv}) 0.928, predictive r^2 (r^2_{pred}) 0.475 and higher contribution of electrostatic field (53.2 %) than steric (46.8 %) field. In order to improve the predictive power of the model, four compounds whose residual

values were on higher side were considered as outliers **(Compounds 6, 19, 29, 49 and 50)** and subsequent analysis (Analysis B) was carried out. The CoMFA model developed yielded cross-validated r^2 (r^2_{cv}) 0.596 at sixth component, non-cross-validated r^2 (r^2_{ncv}) 0.945 with lower standard error of estimate (0.224), predictive r^2 (r^2_{pred}) increased as high as 0.790. A high bootstrapped r^2 of 0.971 adds a high confidence limit to this analysis. In this analysis both steric and electrostatic fields contribute to the QSAR equation by 45.5 % and 54.5 %, respectively, suggesting that variation in biological activity of inhibitors is dominated by differences in electrostatic interactions with the FTase active site. A graph of actual *versus* fitted/predicted activities for training and test set molecules of 3-aminopyrrolidinone derivatives using CoMFA studies is depicted in **Figure 5.3.2.**

2-Aminonicotinonitriles

2-Aminonicotinonitriles developed by Wang et al as farnesyltransferase inhibitors have been used to generate 3D QSAR models initially from 44 compounds in training set **(Table 5.3.2)** and 15 in test set (Analysis A'). But this model displayed high standard error (0.463) and low r^2_{pred} (0.357) values. Hence, in order to improve the predictive power of the model, compounds with higher residual values were removed as outliers **(Compounds 63, 78, 79, 92, 93, 96 and 101).**

A statistically significant model (using Analysis B') was then obtained with cross-validated r^2 (r^2_{cv}) 0.803 with four components, low standard error of prediction (SEP) 0.285, non-cross-validated r^2 (r^2_{ncv}) 0.983 and predictive r^2 (r^2_{pred}) as high as 0.811. The respective steric and electrostatic field contributions were 54.2 % and 45.8 %. A graph of actual *versus* fitted/predicted activities for training/test set molecules is depicted in **Figure 5.3.3.**

Table 5.3.4 Summary of CoMFA results from atom-based rms alignment

Statistical parameters	Alignments					
	I[a]		II[b]		III[c]	
	Analysis A	Analysis B	Analysis A′	Analysis B′	Analysis A″	Analysis B″
r^2_{cv}	0.526	0.596	0.403	0.803	0.346	0.479
N_c	7	6	2	4	11	8
SEP	0.615	0.414	0.463	0.285	0.403	0.422
r^2_{ncv}	0.928	0.945	0.893	0.983	0.998	0.993
SEE	0.251	0.224	0.189	0.089	0.024	0.048
F value	44.587	62.660	180.441	261.653	1112.47	373.34
P $r^2 = 0$	0.0	0.0	0.0	0.0	0.0	0.0
r^2_{pred}	0.475	0.790	0.357	0.811	0.289	0.686
r^2_{bs}	0.967	0.971	0.913	0.988	-	0.996
std dev	0.014	0.013	0.089	0.004	-	0.003
Contrib. S	0.468	0.485	0.455	0.542	0.374	0.389
Contrib. E	0.532	0.515	0.545	0.458	0.626	0.611

[a] 3-Aminopyrrolidinone derivatives; [b] 2-Aminonicotinonitriles; [c] 1-Aryl-1′-imidazolylmethyl ethers

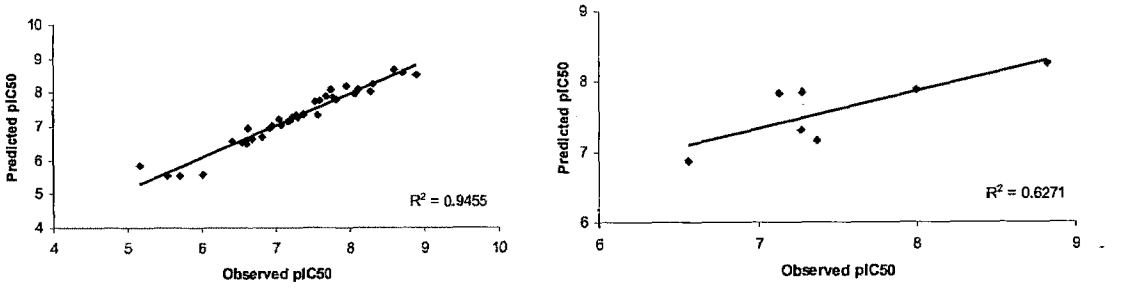

Figure 5.3.2 A graph of actual *versus* fitted/predicted activities for training and test set molecules of 3-aminopyrrolidinones obtained by CoMFA analysis

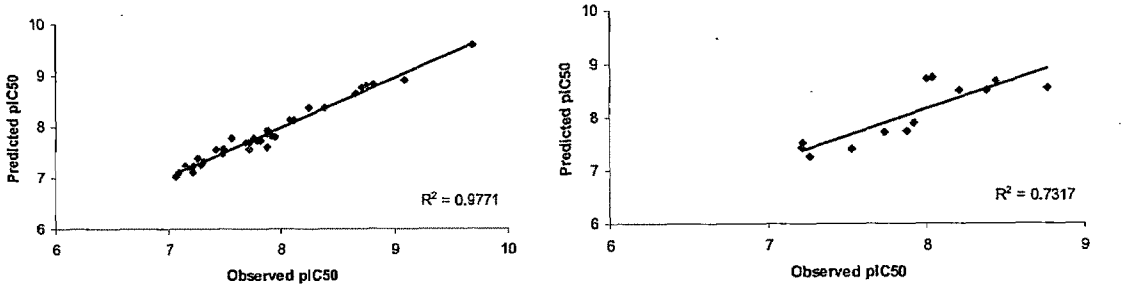

Figure 5.3.3 A graph of actual *versus* fitted/predicted activities for training and test set molecules of 2-aminonicotinonitriles obtained by CoMFA analysis

1-Aryl-1'-imidazolylmethyl ethers

1-Aryl-1'-imidazolylmethyl ether derivatives **(Table 5.3.3)** with selective FTase inhibitory activity developed by cancer research group at Abbott laboratories were used in the generation of 3D QSAR models. Similar to above two structurally diverse classes of FTase inhibitors, initial CoMFA model (using Analysis A") gave significantly poor statistical results with low cross-validated r^2 (r^2_{cv}) 0.346 at eleventh component, high standard error of prediction (SEP) 0.403, F-value erratically rose to 1112.47 and finally the predictive power of the model (r^2_{pred}) was 0.374. After removing outliers **(Compounds 119 and 150)** a CoMFA model was developed from a training set comprising of 30 molecules and validated by 5 test set molecules. A combination of steric and electrostatic fields yielded the CoMFA model having r^2_{cv} 0.479 with eight components, r^2_{ncv} 0.993, predictive r^2 0.686 and exhibited higher electrostatic field contribution (61.1 %). A graph of actual *versus* fitted/predicted activities for training/test set molecules is shown in **Figure 5.3.4.**

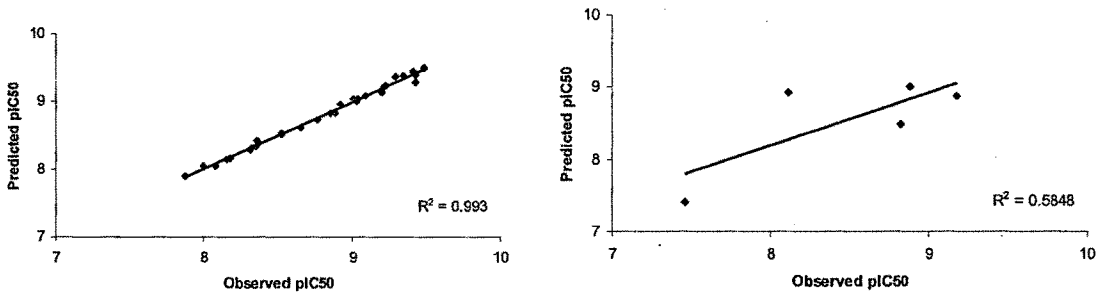

Figure 5.3.4 A graph of actual *versus* fitted/predicted activities for training and test set molecules of 1-aryl-1'-imidazolylmethyl ethers by CoMFA

5.3.2.2 COMSIA models

To investigate the significance of hydrophobic and H-bond fields on the FTase inhibitory activity, CoMSIA analysis using steric, electrostatic, hydrophobic and H-bond fields were carried out for all the three sets of benzonitrile derivatives. The

compounds which were removed as ouliers in CoMFA studies were not included in the CoMSIA analysis. In the results summarized for CoMSIA analysis, steric and electrostatic fields are not reported individually as the statistical results and position of contour maps did not vary significantly from that of CoMFA.

3-Aminopyrrolidinone derivatives

The results of CoMSIA PLS analysis are summarized in **Table 5.3.5.** The CoMSIA models generated from steric and electrostatic fields did not vary both in terms of statistical values and positions of contours as compared to its CoMFA model and hence are not included in the table.

A statistically significant and robust model (Model 2) was obtained. The combinations of steric, electrostatic, H-bond donor and acceptor fields and hydrophobic fields yielded CoMSIA models with an improved r^2_{cv} 0.469 with eight components, highest predictive value of r^2 0.787, r^2_{ncv} 0.923, r^2_{bs} 0.969 with steric (12.2 %), electrostatic (21.1 %), hydrophobic (12.7 %), H-bond donor (23.4 %) and acceptor (30.6 %) field contributions. The 3D contour maps analyzed using Model 2 are shown in **Figures 5.3.8(C), 5.3.9 and 5.3.10.** The graph of actual *versus* fitted/predicted activities for training/test set molecules is depicted in **Figure 5.3.5.** These CoMSIA studies signify the contribution of H-bond donor, acceptor and hydrophobic fields in addition to steric and electrostatic fields toward the FTase inhibitory activity of 3-Aminopyrolidinones.

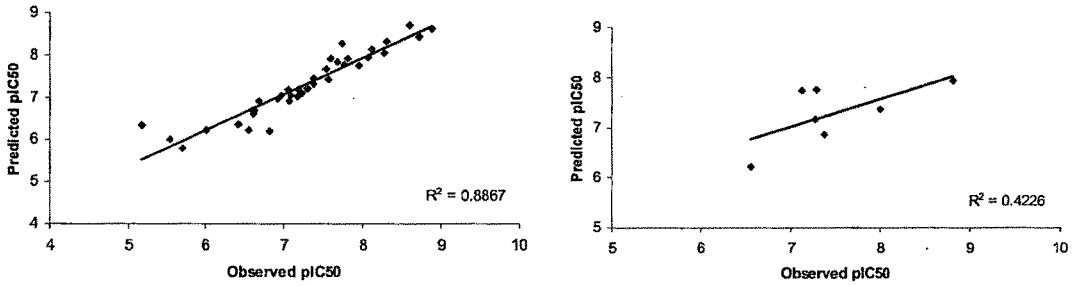

Figure 5.3.5 A graph of actual *versus* fitted/predicted activities for training and test set molecules of 3-aminopyrrolidinones obtained by CoMSIA analysis

Table 5.3.5 Summary of CoMSIA results for 3-Aminopyrrolidinone derivatives

Statistical parameters	Model							
	1	2	3	4	5	6	7	8
	HDA	**SEDAH**	SDAH	SDH	SDA	SEA	SEDA	SEDH
r^2_{cv}	0.313	**0.469**	0.256	0.330	0.419	0.290	0.300	0.451
N_c	7	**8**	7	8	8	9	4	8
SEP	0.724	**0.648**	0.754	0.728	0.678	0.763	0.696	0.659
r^2_{ncv}	0.898	**0.923**	0.914	0.922	0.846	0.904	0.713	0.938
SEE	0.280	**0.247**	0.261	0.248	0.249	0.280	0.445	0.222
F value	36.33	**41.88**	37.18	41.34	19.21	28.26	19.91	52.75
P $r^2 = 0$	0.0	**0.0**	0.0	0.0	0.0	0.0	0.0	0.0
r^2_{pred}	0.653	**0.787**	0.646	0.688	0.606	0.516	0.665	0.534
r^2_{bs}	0.925	**0.962**	0.952	0.967	0.897	0.955	0.843	0.960
S.D	0.025	**0.023**	0.028	0.016	0.026	0.023	0.061	0.011
Contribution (fractions)								
S	-	**0.122**	0.151	0.559	0.270	0.233	0.161	0.154
E	-	**0.211**	-	-	-	0.376	0.301	0.294
H	0.461	**0.306**	0.381	0.219	-	-	-	0.401
D	0.186	**0.127**	0.157	0.222	0.232	-	0.112	0.151
A	0.353	**0.234**	0.311	-	0.498	0.390	0.426	-

S = steric, E = electrostatic, D = H-bond donor, A = H-bond acceptor, H = hydrophobic

Incorporation of the H-bond donor and acceptor fields yielded model 7 with predictive r^2 value of 0.665. This model showed comparable predictions, but the standard error was on a higher side and also the cross-validated r^2 was low (0.30). Hence, the model was considered to be of less statistical significance. Further hydrophobic fields were incorporated in order to study its influence on the model.

2-Aminonicotinonitriles

The results of PLS analysis for CoMSIA are summarized in **Table 5.3.6.** Model III generated from steric, hydrophobic, H-bond donor and acceptor fields showed r^2_{cv} 0.705 with five components, the corresponding r^2_{ncv} as 0.868 and predictive r^2 0.757. Model VIII generated using steric, electrostatic, hydrophobic and H-bond donor exhibited significant contribution of hydrophobic and electrostatic fields with improved statistical correlation coefficients r^2_{cv} 0.827, r^2_{ncv} 0.939 and predictive r^2 0.695. Further, model VII obtained with the combination of steric, electrostatic, H-bond donor and acceptor fields showed r^2_{cv} 0.806, r^2_{ncv} 0.974 and predictive r^2 of 0.747.

Model II generated using all five CoMSIA fields yielded statistically significant model with r^2_{cv} 0.814 for five components, r^2_{ncv} 0.931, r^2_{bs} 0.949 and r^2_{pred} 0.784 and respective field contributions were steric 8.5 %, electrostatic 30.6 %, hydrophobic 21.4 %, H-bond donor 18.7 % and acceptor 20.7 %. This model with good internal and external predictions was used to analyze 3D contour plots **[Figures 5.3.11(C), 5.3.12, 5.3.13]**. The plot depicting actual *versus* fitted/predicted activities of data set molecules is shown in **Figure 5.3.6.** The analysis of model II showed higher contributions of hydrophobic and electrostatic fields to the FTase inhibitory activity of 2-aminonicotinonitrile derivatives.

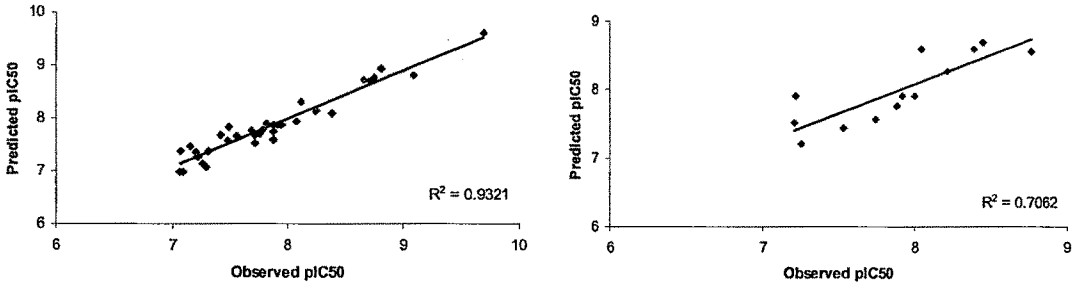

Figure 5.3.6 A graph of actual *versus* fitted/predicted activities for training and test set molecules of 2-aminonicotinonitriles obtained by CoMSIA analysis

Table 5.3.6 Summary of CoMSIA results for 2-aminonicotinonitriles

Statistical parameters	Model							
	I	**II**	III	IV	V	VI	VII	VIII
	HDA	**SEDAH**	SDAH	SDH	SDA	SEA	SEDA	SEDH
r^2_{cv}	0.747	**0.814**	0.705	0.628	0.651	0.718	0.806	0.827
N_c	10	**5**	5	4	4	4	4	5
SEP	0.350	**0.280**	0.353	0.392	0.380	0.341	0.283	0.271
r^2_{ncv}	0.958	**0.931**	0.868	0.790	0.754	0.927	0.874	0.939
SEE	0.143	**0.171**	0.236	0.294	0.318	0.174	0.228	0.102
F value	79.17	**101.18**	52.74	38.59	31.45	130.01	71.04	100.26
P $r^2 = 0$	0.0	**0.0**	0.0	0.0	0.0	0.0	0.0	0.0
r^2_{pred}	0.724	**0.784**	0.757	0.570	0.627	0.634	0.747	0.695
r^2_{bs}	0.976	**0.939**	0.896	0.822	0.764	0.937	0.885	0.948
std dev	0.010	**0.019**	0.032	0.031	0.037	0.016	0.027	0.014
Contribution (fractions)								
S	-	**0.085**	0.133	0.269	0.220	0.102	0.112	0.122
E	-	**0.306**	-	-	-	0.517	0.371	0.439
H	0.487	**0.214**	0.324	0.527	-	-	-	0.285
D	0.092	**0.187**	0.217	0.204	0.229	-	0.209	0.154
A	0.422	**0.207**	0.326	-	0.551	0.320	0.308	-

S = steric, E = electrostatic, D = H-bond donor, A = H-bond acceptor, H = hydrophobic

1-Aryl-1'-imidazolylmethyl ethers

Table 5.3.7 summarizes the results of CoMSIA PLS analysis for 1-aryl-1'-imidazolyl methyl ethers. Model 'E' generated from the steric, electrostatic and H-bond donor fields exhibited better predictions with r^2_{cv} 0.392 at eight components, r^2_{ncv} 0.934 and predictive r^2 0.342. Model 'G' generated using combination of steric, electrostatic, H-bond donor and acceptor fields yielded statistically significant model as compared to all other combinations and exhibited r^2_{cv} 0.444 with eight components, r^2_{ncv} 0.984 and predictive r^2 0.400. The 3D contours analyzed for Model 'G' are shown in **Figures 5.3.14(C)** and **5.3.15**. The graph of actual *versus* fitted/predicted activities for training/test set molecules is depicted in **Figure 5.3.7**. The models derived from other combinations like SDH, SEDH, HAD resulted in poor r^2_{pred} values and were considered to be of poor statistical significance. FTase inhibitory activity of 1-aryl-1'-imidazolyl methyl ethers was found to be contributed significantly by H-bond acceptor and electrostatic fields.

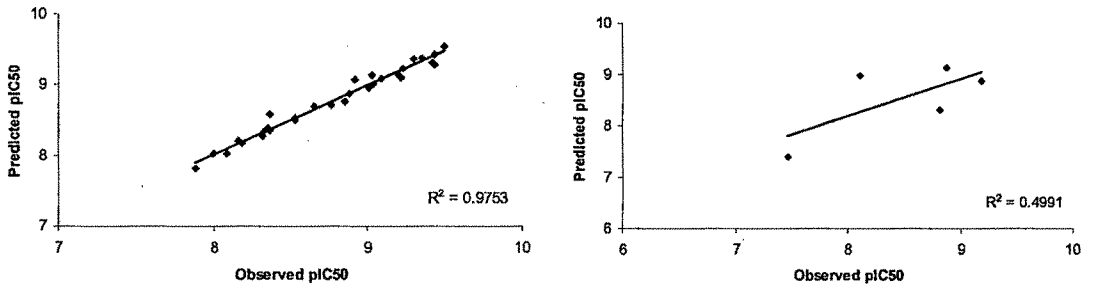

Figure 5.3.7 A graph of actual *versus* fitted/predicted activities for training and test set molecules of 1-aryl-1'-imidazolylmethyl ethers by CoMSIA

Table 5.3.7 Summary of CoMSIA results for 1-aryl-1'-imidazolylmethyl ethers

Statistical parameters	Model							
	A	B	C	D	E	F	G	H
	HDA	SEDAH	SDAH	SDH	SED	SEA	**SEDA**	SEDH
r^2_{cv}	0.124	0.382	0.382	0.284	0.392	0.357	**0.444**	0.338
N_c	2	6	10	6	8	7	8	7
SEP	0.477	0.434	0.478	0.467	0.451	0.454	**0.411**	0.460
r^2_{ncv}	0.443	0.988	0.995	0.916	0.934	0.973	**0.984**	0.968
SEE	0.380	0.065	0.042	0.160	0.149	0.092	**0.074**	0.101
F value	10.73	181.10	388.45	41.99	36.903	114.93	**158.62**	95.033
P $r^2 = 0$	0.0	0.0	0.0	0.0	0.0	0.0	**0.0**	0.0
r^2_{pred}	0.113	0.345	0.384	0.281	0.342	0.343	**0.399**	0.106
r^2_{bs}	0.624	0.997	0.996	0.957	0.968	0.991	**0.989**	0.986
S.D	0.145	0.002	0.005	0.025	0.022	0.005	**0.006**	0.007
Contribution (fraction)								
S	-	0.183	0.108	0.378	0.321	0.168	**0.093**	0.189
E	-	0.513	-	-	-	0.458	**0.266**	0.488
H	0.328	0.299	0.190	0.619	-	-	-	0.319
D	0.069	0.005	0.003	0.003	0.002	-	**0.008**	0.008
A	0.602	0.190	0.221	-	0.677	0.375	**0.219**	-

5.3.2.2 Graphical Interpretation of the CoMFA and CoMSIA Models

The steric contour maps indicate green and yellow contours as sterically favorable and unfavorable areas. Blue and red contours in the electrostatic maps indicate areas where positive and negative charge substituent's favor activity. Hydrophobic, H-bond donor and acceptor contour maps indicate favorable yellow, cyan, magneta contours and disfavorable by white, violet/purple and red contours, respectively. Although, the contour maps cannot be used as receptor maps but useful interpretations can be derived from them. The generated contour maps were mapped on the FTase active site, and fields were analyzed with respect to the amino acid residues of FTase. To aid in visualization, the template molecule in each class of compounds is displayed in the respective figures and the contour maps are discussed with the reference compound.

3-Aminopyrrolidinones

Figure 5.3.8(A) and 5.3.8(B) corresponds to the CoMFA steric and electrostatic contour maps for 3-aminopyrolidinones with the active molecule (compound **47**). The green contour observed in the vicinity of chlorine suggests that steric substituents in these regions may favor activity (compounds **22, 24, 35**), while the disfavored yellow contours in the vicinity of nitrogen attached to pyrrolidinone and tert.butoxycarbonylamino propyl group restrict steric substitution indicating decreased biological activity (compounds **37-41**). In the CoMFA electrostatic map, the red contour surrounding chlorine on ring 'X' indicates the significance of negatively charged/electron rich group for biological activity (compounds **46, 47** and **48**). It was clearly observed that if 'X' ring is unsubstituted, the biological activity tends to decrease (compounds **37-44**). The blue contour overlapping the cyano group of ring 'Y' indicates the significance of positively charged group for biological activity.

CoMFA steric and electrostatic contour plots mapped on FTase active site are depicted in **Figures 5.3.8(A) and (B)** with highest active compound **47** in orange and lowest active compound **31** in violet, respectively. The sterically favored green contour was placed in between His 248 and Tyr251, while disfavored yellow contours were observed at the periphery of Tyr365, Arg202 and overlapping phenyl ring of Phe253. The orientation of pyrridinone ring towards zinc may be one of the major reasons why compound **47** is more active as the possibility of pyrrolidinone ring oxygen forming bond with zinc is higher, which is not the case with the least active compound **31**.

The positively charged favored blue contour near the cyano substituent on ring 'Y' was placed close to Arg202 and Trp303, while, small negatively charged red contour was observed near Val201, Asp297 and His248. 4-Cl may have van der Waals contact with Try 251.

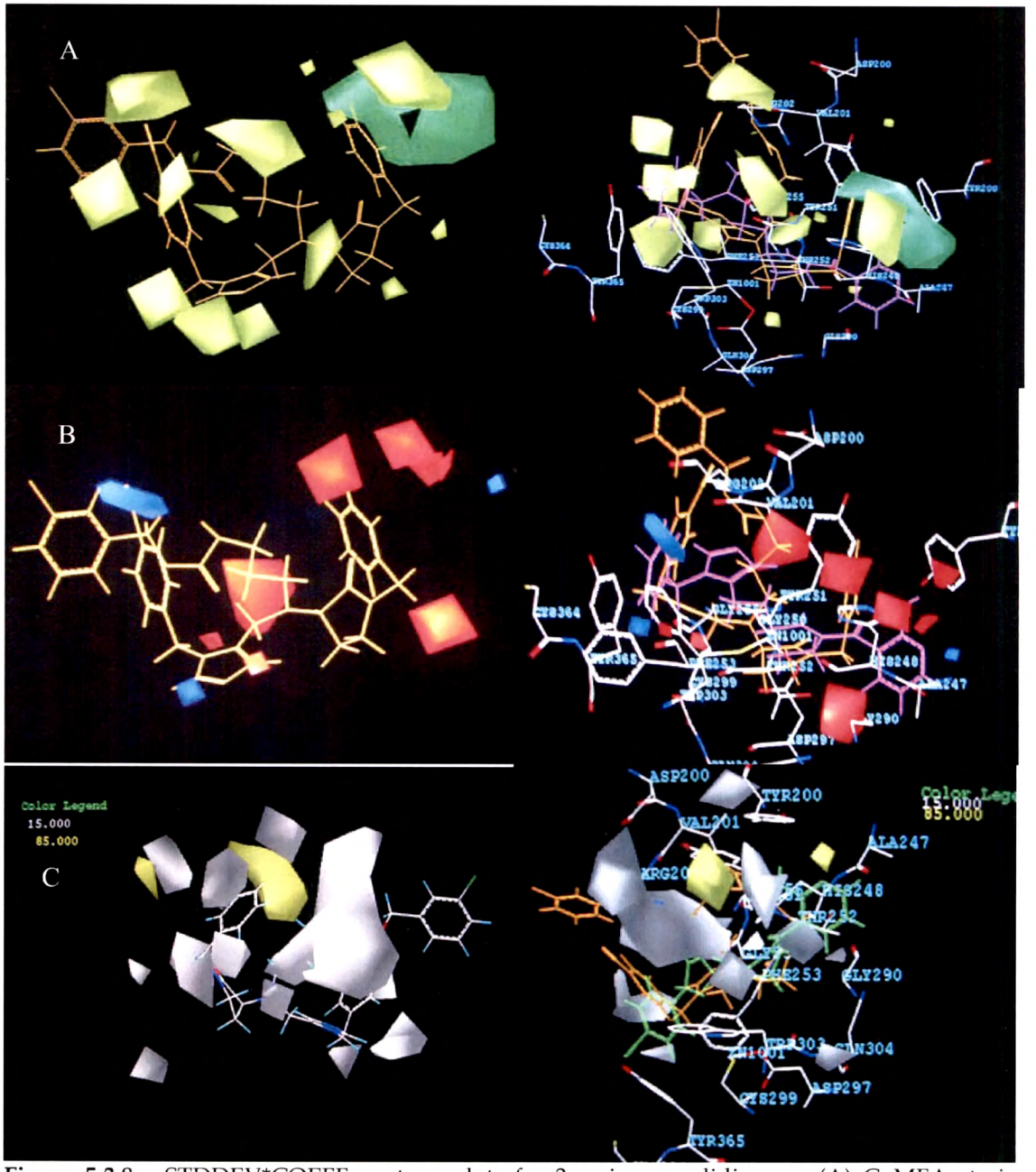

Figure 5.3.8 STDDEV*COEFF contour plots for 3-aminopyrrolidinones. (A) CoMFA steric (green polyhedron: sterically favored; yellow polyhedron: sterically disfavored) and their superimposition on FTase active site. (B) CoMFA electrostatic (red polyhedron: negatively charged favored; blue polyhedron: positively charged favored) maps and their superimposition on FTase active site. (C) CoMSIA hydrophobic (yellow polyhedra: favored hydrophobic substituents; white polyhedra: disfavored hydrophobic substituents) contours and their superimposition on FTase active site. Compound **47** (orange) the most active and compound **31** (least active) is shown in violet, purple and green in A, B, C respectively.

Figure 5.3.8(C) displays the CoMSIA hydrophobic contour maps and their overlapping on the FTase active site with compound **47**. The hydrophobic contour plots connotate disfavored large white regions in the vicinity of rings 'X' and 'Y', which are found overlapping on Arg202. Also small disfavored white contours are seen overlapping the tert.butoxycarbonylamino substituent near Thr252 and Phe253, which indicate that optimum lipophilic substituents may decrease or enhance the biological activity. Favored yellow region in the vicinity of benzyl group indicate the significance of lipophilic substituents for biological activity. The CoMSIA steric and electrostatic contour maps appear in the same region as that of CoMFA and hence are not discussed here.

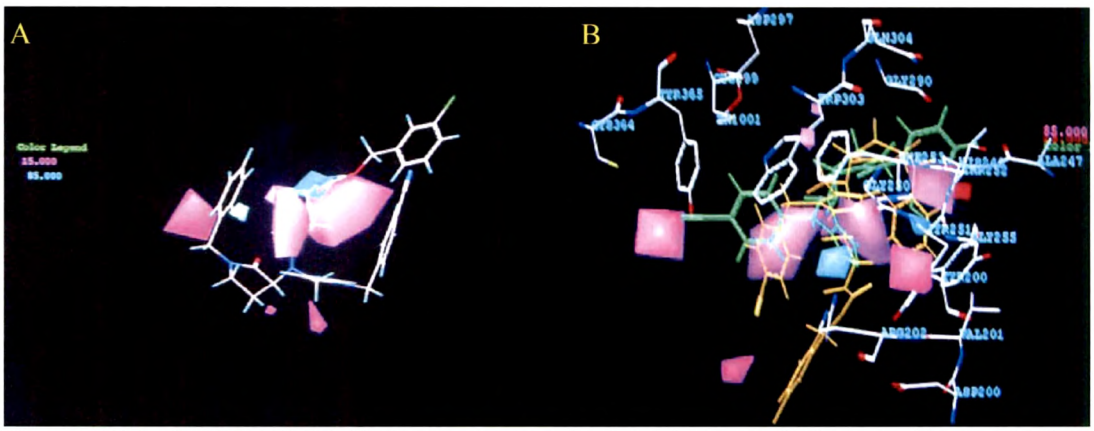

Figure 5.3.9 STDDEV*COEFF contour plots for 3-aminopyrrolidinones. (A) CoMSIA H-bond donor contours with compound **47**. (B) CoMSIA H-bond donor contour maps superimposed on FTase active site.

CoMSIA H-bond donor contour maps are displayed in **Figure 5.3.9(A)**. H-bond donor favoring cyan contour was observed near –NH of tert.butoxycarbonylamino substituent of compound **47**, indicating that H-bond donor groups in this region may favor activity (compounds **44 and 48**). Further, compounds which lack H-bond donor substituents in these regions showed decreased activity (compounds **1-5, 7-12**). Unfavorable purple contours were observed close to benzyl attached to pyrrolidinone and on the planar surface near the carbonyl amide linkage of compound **47**.

H-bond acceptor contour maps **(Figure 5.3.10)** show favorable magneta contours in the vicinity of carbonyl and cyano group of compound **47** indicating its significance for biological activity.

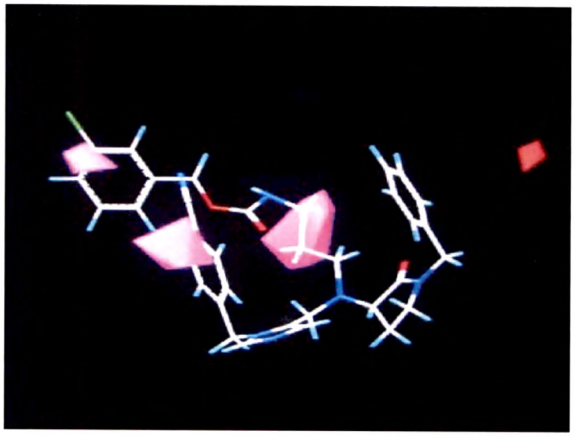

Figure 5.3.10 CoMSIA H-bond acceptor contour plots for 3-aminopyrrolidinones with compound **47.**

2-Aminonicotinonitriles

The CoMFA steric and electrostatic contour plots with the template molecule (compound **97**) and its superimposition on the FTase active site are shown in **Figures 5.3.11(A) and (B)**. The hydrophobic contour map and its superimposition on the FTase active site is displayed in **Figure 4.6.10 (C)**.

The CoMFA steric plot portraying sterically favoring green polyhedra near to the napthyl ring suggests that optimum steric substituents in this region favor activity (compounds **105, 112**). Sterically disfavored yellow contours were observed in the vicinity of –CN group of ring 'A' indicating restriction for incorporating bulky steric substituents which may decrease FTase inhibitory activity.

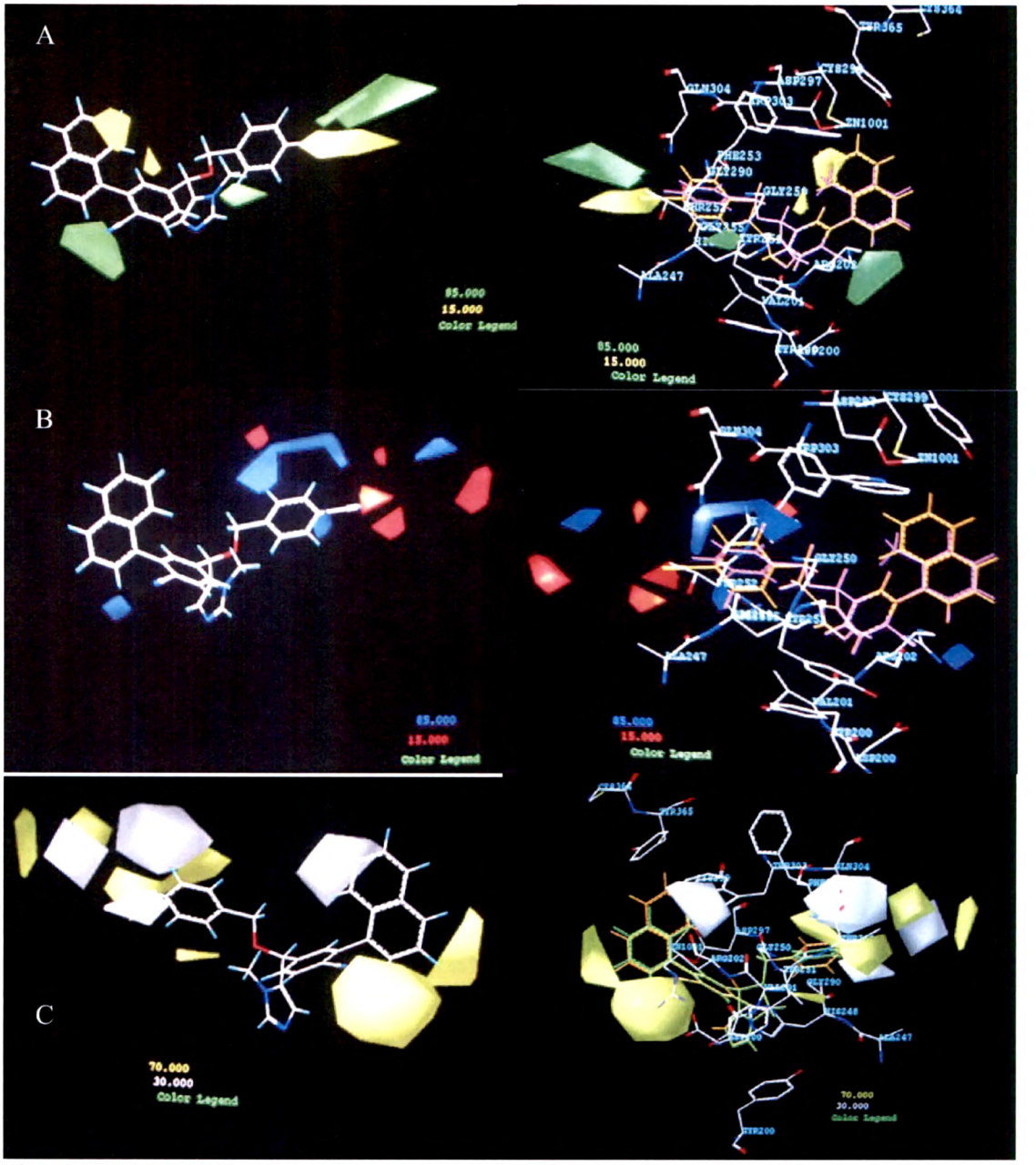

Figure 5.3.11 STDDEV*COEFF contour plots for 2-aminonicotinonitriles. (A) CoMFA steric contours and their superimposition on FTase active site. (B) CoMFA electrostatic maps and their superimposition on FTase active site. (C) CoMSIA hydrophobic contours and their superimposition on FTase active site. Compound **97** (orange) the most active and compound **51** (least active) is shown in violet, purple and green in A, B, C, respectively.

CoMFA electrostatic contour plots displayed a positively charged favored large blue contour surrounding ring 'A' signifying that an increase in activity may be due to low

electron density substituents, while small negatively charged favored red contours near 4-CN (ring A) specify that the electron rich substituents favor activity (compounds **61, 98-100, 102**). Moderate activity was observed for compounds **64** and **76**.

Figures 5.3.11(A) and (B) portray mapping of CoMFA steric and electrostatic contour maps on the active site of farnesyltransferase. The sterically favored green contour is seen placed at the periphery of Arg202 and also close to Gly255 and Tyr251, while disfavored yellow contours were seen close to zinc and Thr252. The positively charged favored blue contour surrounding ring 'A' was observed overlapping over Gly290. The small negatively charged red contour on the upper part of 4-CN on ring 'A' was observed near Thr252 where 4-CN might have van der Waals contact.

The CoMSIA steric and electrostatic contour maps and their mapping on FTase active site are displayed in **Figure 5.3.12(A) and (B),** respectively with compound **97**. In the steric contour map a large favorable green contour was observed near ring 'A', suggesting that steric substituents in this region favor activity (compounds **61, 76, 103-111**). These contours are seen overlapping Gln304 and close to Trp303. Sterically unfavorable yellow contour placed near Tyr365 was observed close to the methyl substituent on the five membered ring indicating restricted area for bulkier substituents. This may be one of the reasons for poor biological activity of compound **31** (shown in purple). CoMSIA electrostatic contour maps are not discussed as they were similar to those observed in CoMFA.

Figure 5.3.11(C) displays the CoMSIA hydrophobic contour map and its superimposition on the FTase active site with highest active compound **97**. In the hydrophobic contour map, favorable yellow contours were observed in the vicinity of cyano group of ring 'A', 'B' and napthyl ring where increased lipophilic substituents may favor activity (compounds **98-102**), while, disfavored white contours were seen in the vicinity of napthyl ring and ring 'A' indicating regions where hydrophilic

substituents may enhance activity and lipophilic substituents may decrease activity (compounds **85- 87**).

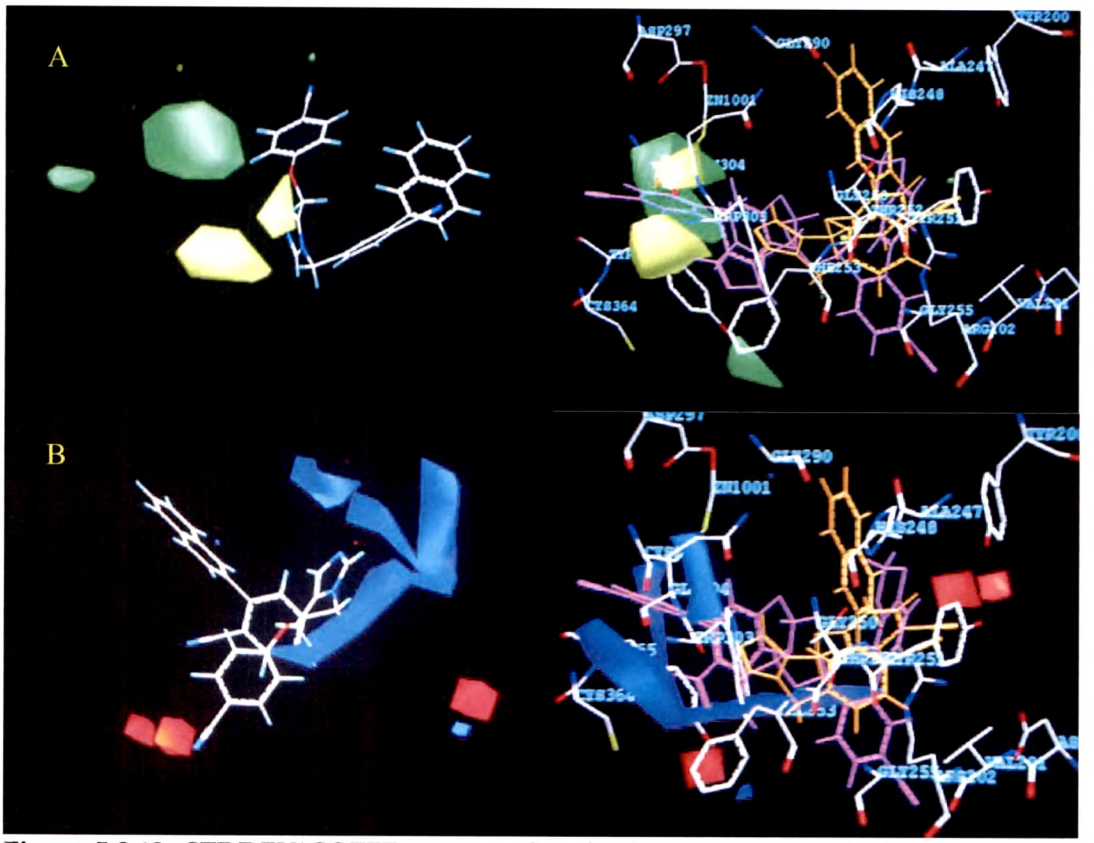

Figure 5.3.12 STDDEV*COEFF contour plots for 2-aminonicotinonitriles. (A) CoMSIA steric contour maps with compound **97** and its superimposition on FTase active site. (B) CoMSIA electrostatic contour maps with compound **97** and its superimposition on FTase active site.

The hydrophobic contour plots which connotate disfavored white regions close to naphthyl ring and ring 'A' occupy space between Zinc-Cys299 and Gln304-Thr302, respectively while, favored yellow contours are seen in the periphery of Asp300 and surrounding Thr252. **Figure 5.3.13** displays CoMSIA H-bond donor contour maps. The CoMSIA H-bond donor contour map depicts large favorable cyan contours adjacent to ring 'A' and parallel to ring 'B' in the vicinity of napthyl ring signifying the presence of H-bond donor groups in these regions for FTase inhibitory activity (compounds **91, 95** and **102**).

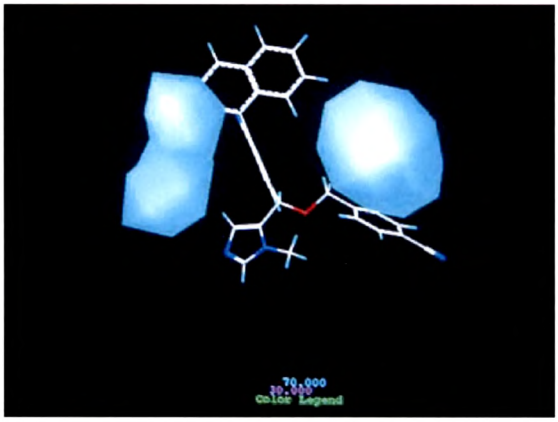

Figure 5.3.13 CoMSIA H-bond donor contour map for 2-aminonicotinonitriles with compound **97**.

This can be considered as one of the reasons why Wang and his co-researchers[12] considered cyano group as an optimum para substituent on both rings 'A' and 'B' throughout the series of compounds synthesized for FTase inhibitory activity.

1-Aryl-1'-imidazolylmethyl ethers

Figures 5.3.14(A) and (B) correspond to the CoMFA steric and electrostatic contour maps and their mapping on FTase active site for 1-aryl-1'-imidazolylmethyl ethers with the active molecule (compound **152**).

The large green contour observed in the vicinity of ring 'C' suggests that steric substituents in this region may favor higher activity (compounds **127, 131, 141, 142, 143, 151**). The green contour was observed near to Arg202 and one more sterically favorable small green contour occupied space between Cys364 and Cys299 overlapping Try302. The disfavored yellow contour surrounding the imidazole ring restricts steric substitution indicating decreased biological activity. It was found placed close to zinc and Trp303.

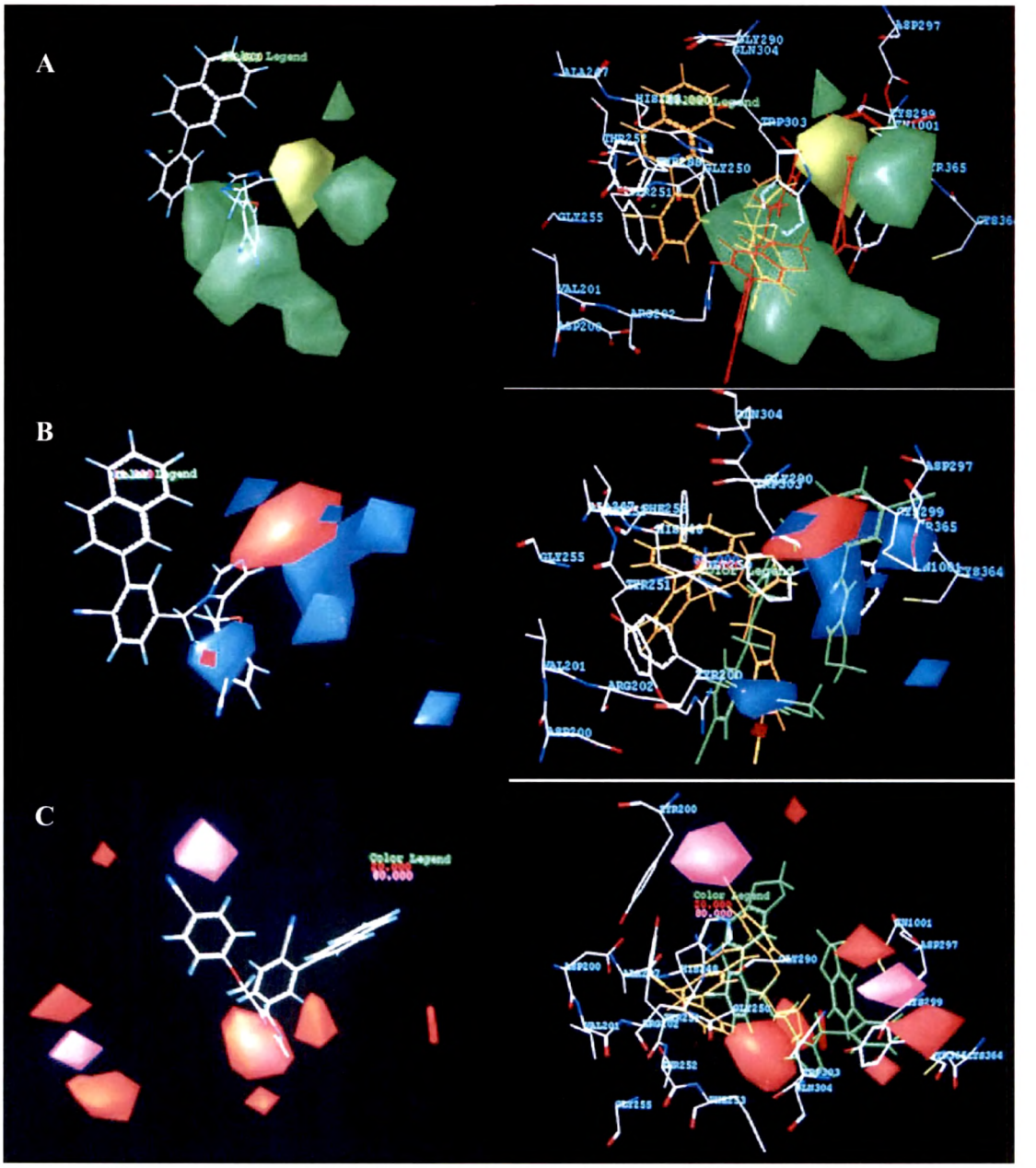

Figure 5.3.14 STDDEV*COEFF contour plots for 1-aryl-1'-imidazolylmethyl ethers. (A) CoMFA steric contours and their superimposition on FTase active site. (B) CoMFA electrostatic maps and their superimposition on FTase active site. (C) CoMSIA H-bond acceptor contours and their superimposition on FTase active site. Compound **152** (orange) the most active and compound **145** (least active) is shown in red, green and green in A, B, C respectively.

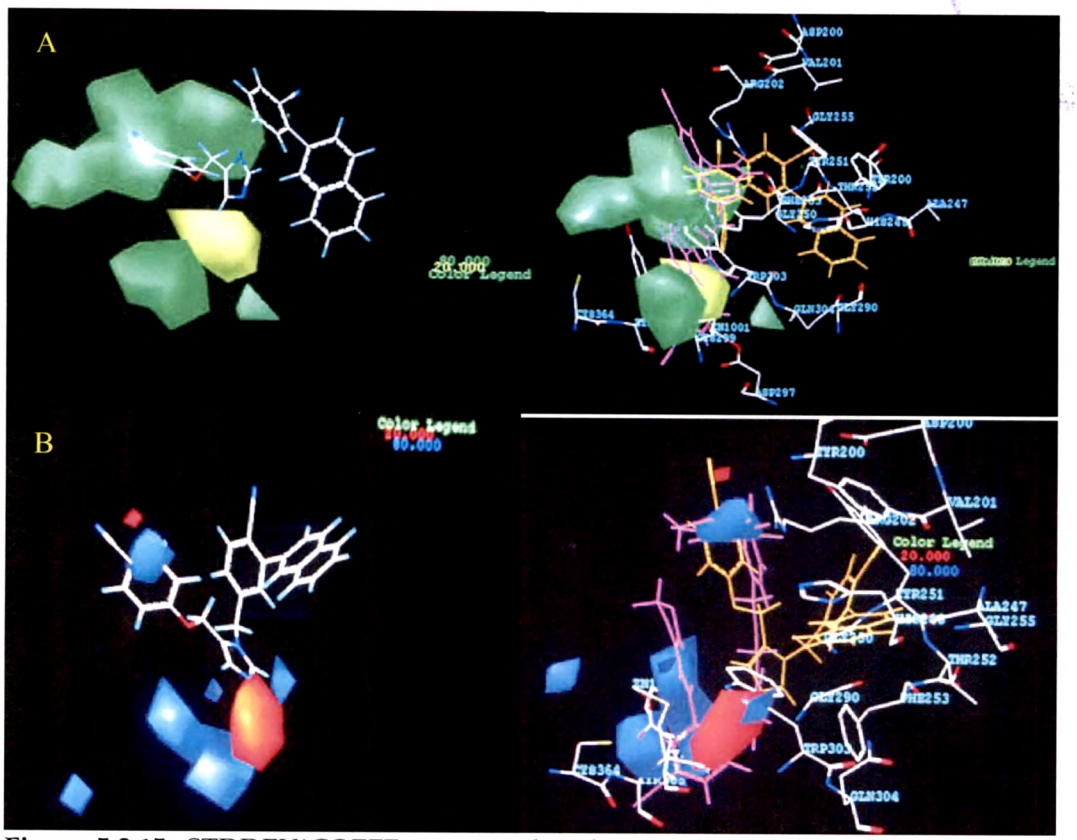

Figure 5.3.15 STDDEV*COEFF contour plots for 1-aryl-1'-imidazolylmethyl ethers. (A) CoMSIA steric contour maps with compound **152** and its superimposition on FTase active site. (B) CoMSIA electrostatic contour maps with compound **152** and its superimposition on FTase active site.

In the CoMFA electrostatic map, blue contour embedded in ring 'C' indicates the significance of positively charged group for farnesyltransferase inhibitory activity (compounds **127, 130, 131**) which was observed in the periphery of Cys299, Tyr365 and zinc, while small negatively charged favored red contour near imidazole nucleus specify that electron rich substituents favor activity.

Not much significant difference in the position of CoMSIA steric and electrostatic contour maps were observed as compared to CoMFA, but these steric and electrostatic contour maps and their superimposition on FTase active site is depicted in **Figures 45.3.15(A) and (B)**.

CoMSIA H-bond acceptor contours and their overlapping on FTase active site are displayed in **Figure 5.3.14(C)** with compound **152**. The H-bond acceptor contour maps show favorable magneta contours in the vicinity of para cyano group of ring 'C' near to Tyr200 signifying the presence of electronegative groups for biological activity (compounds **117, 118, 123, 124, 130**), while small disfavorable red contours embedded in imidazole ring and in the vicinity of ortho substitution on ring 'D' restricts substitution of H-bond donor groups which may decrease the biological activity. The disfavorable red contours occupied space in the vicinity of Gly250, Trp303 and Gln304. It can be observed that p-cyano group of ring 'C' orients towards favored magneta contour in case of compound **152** with potent inhibitory activity, while this is not the case with **145** (shown in green) as it has orientation which does not favor FTase inhibitory activity.

Table 5.3.8 CoMFA *versus* CoMSIA

Statistical parameters	Alignments					
	I[a]		II[b]		III[c]	
	CoMFA	CoMSIA	CoMFA	CoMSIA	CoMFA	CoMSIA
r^2_{cv}	0.596	0.469	0.803	0.814	0.479	0.411
N_c	6	8	4	5	8	8
SEP	0.414	0.648	0.285	0.280	0.422	0.444
r^2_{ncv}	0.945	0.923	0.983	0.931	0.993	0.984
SEE	0.224	0.247	0.089	0.171	0.048	0.074
F value	62.660	41.883	261.653	101.184	373.34	158.62
P $r^2 = 0$	0.0	0.0	0.0	0.0	0.0	0.0
r^2_{pred}	0.790	0.787	0.811	0.784	0.686	0.399
r^2_{bs}	0.971	0.962	0.988	0.939	0.996	0.989
std dev	0.013	0.023	0.004	0.019	0.003	0.006

[a]3-Aminopyrrolidinone derivatives; [b]2-Aminonicotinonitriles; [c]1-Aryl-1'-imidazolylmethyl ethers

Comparison of the statistical results of the best models obtained by CoMFA and CoMSIA are summarized in **Table 5.3.8.** In all the three series CoMFA yielded better statistically significant and predictive models as compared to CoMSIA. Predictive r^2

values were as high as 0.811 which clearly highlights the predictive power of the CoMFA models developed. In case of 2-aminonicotinonitriles, the CoMSIA calculated cross-validated r^2 value was slightly more than the CoMFA, but the predictive r^2 value was on lower side as compared to CoMFA.

5.4 References

1. Wang, L.; Wang, G. T.; Wang, X.; Tong, Y.; Sullivan, G.; Park, D.; Leonard, N. M.; Cohen, J.; Gu, W.Z.; Zhang, H.; Bauch, J. L.; Jakob, C. G.; Hutchins, C. W.; Stoll, V. S.; Marsh, K.; Rosenberg, S. H.; Sham, H. L and Lin, N-H. *J. Med. Chem.* **2004**, 47, 612.
2. Mallams, A. K.; Rossman, R. R.; Doll, R. J.; Girijavallabham, V. J.; Ganguly, A. K.; Petrin, J.; Wang, L.; Patton, R.; Bishop, R.; Carr, D. M.; Kirschmacher, P.; Catino, J. J.; Bryant, M. S.; Chen, K-J.; Korfmacher, W. A.; Nardo, C.; Wang, S.; Nomier, A. A.; Lin,C-C.; Jianping, C.; Lee, S.; Dell, J.; Lipari, P.; Malkowski, M.; Yaremko, B.; King, I and Liu, M. *J. Med. Chem.* **1998**, 41, 877.
3. Bell, I. M.; Gallicchio, S. N.; Abrams, M.; Beshore, D. C.; Buser, C. A.; Culberson, J. C.; Davide, C.; Hutchings, M.; Fernandes, C.; Gibbs, J. B.; Graham, S. L.; Hartman, G. D.; heimbrook, D. C.; Homnik, C. F.; Huff, J. R.; Kassahun, K.; Koblan, K. S.; Kohl, N. E.; Lobell, R. B.; Lynch, J. L.; Miller, P. A.; Omer, C. A.; Rodrigues, D.; Walsh, E. S and Williams, T. M. *J. Med. Chem.* **2001**, 41, 2033.
4. Wang, G. T.; Wang, X.; Wang, W.; Hasvold, L. A.; Sullivan, G.; Hutchins, C. W.; O'Conner, S.; Gentiles, R.; Sowin, T.; Cohen, J.; Gu, W-Z.; Zhang, H.; Rosenberg, S. H and Sham, H. L. *Bioorg. Med. Chem. Lett.* **2004**, 14, 5371.
5. Li, Q.; Wang, G. T.; Li, T.; Gwaltney, S. L.; Woods, K. W.; Claiborne, A.; Wang, X.; Gu, W.; Cohen, J.; Stoll, V. S.; Hutchins, C.; Frost, D.; Rosenberg, S. H and Sham, H. L. *Bioorg. Med. Chem. Lett.* **2005**, 15, 153.